AN ABSTRACT OF THE THESIS OF

Yisen Guo for the degree of Master of Science in Civil Engineering presented on September 7, 2011.

Title: Assessing the Seismic Performance of Corroding RC Bridge Columns.

Abstract approved: _____

David Trejo

Corrosion of reinforcement is recognized as the predominant factor that limits the service life of reinforced concrete (RC) structures exposed to aggressive environments. This corrosion deterioration can lead to damage resulting in capacity loss or even failure. For structures exposed to coastal marine environments or deicing or anti-icing applications, this deterioration is often accelerated.

The corrosion deterioration in RC structures has raised significant attention from researchers and analytical studies and experimental tests have been performed worldwide. Durability and serviceability of corroded RC structures have been investigated to determine the relationship between the corrosion process and the service life of these structures and these relationships have been used to develop service life models. Corrosion of the reinforcement could be especially detrimental to the seismic performance of bridge structures and limited efforts have been made to model the structural performance of RC structures exhibiting corrosion during seismic events. The objective of this paper is to first develop a realistic corrosion rate model that represents actual corrosion conditions and then, using this model, develop another model to predict

the time-variant seismic performance of RC bridge columns exhibiting corrosion of the steel reinforcement. This information can then be used to optimize design, maintenance, repair, and/or replacement of RC bridges.

The service life of RC structures subject to corrosion is comprised of two general phases: the initiation and the propagation phases. Significant efforts have been made in modeling the corrosion initiation phase, but much less efforts have focused on the propagation phase. Different prediction models have been developed to simulate the corrosion process, including empirical models, numerical models (finite element method, boundary element method, and resistor networks and transmission line approach), and analytical models (Otieno et al. 2011). This study provides a critical review of existing models used to predict the corrosion propagation of steel in RC structures. This review is followed by the development of a new model that incorporates critical parameters for modeling the corrosion propagation phase. The new model is based on the physical process and is calibrated with a set of measured long-term field data. This new model is then used to predict corrosion deterioration of a RC column. The column is then analyzed for seismic performance at different states. A reliability analysis of the lateral capacity of the column is then performed. The example column is for a typical highway bridge built in Oregon during the 1970s.

Assessing the Seismic Performance of Corroding RC Bridge Columns

by
Yisen Guo

A THESIS

submitted to

Oregon State University

in partial fulfillment of
the requirements for the
degree of

Master of Science

Presented September 7, 2011
Commencement June 2012

Master of Science thesis of <u>Yisen Guo</u> presented on <u>September 7, 2011.</u>

APPROVED:

_____

Major Professor, representing Civil Engineering

_____

Head of the School of Civil & Construction Engineering

_____

Dean of the Graduate School

I understand that my thesis will become part of the permanent collection of Oregon State University libraries. My signature below authorizes release of my thesis to any reader upon request.

_____

Yisen Guo, Author

ACKNOWLEDGMENTS

First, I would like to express my sincere appreciation to Dr. David Trejo for his guidance and encouragement serving as my graduate advisor. It has been a pleasure to be his student. I also would like to thank the committee members Dr. Michael H. Scott, Dr. Solomon C. Yim, and Dr. Lech Muszynski for their helpful comments and feedback.

Many thanks are owed to my fellow graduate students whose friendship has made my graduate experience more enjoyable.

Finally, I would like to thank my parents and my wife for their love and support.

TABLE OF CONTENTS

LIST OF FIGURES

LIST OF TABLES

Assessing the Seismic Performance of Corroding RC Bridge Columns

INTRODUCTION

Corrosion of reinforcement is recognized as the predominant factor that reduces the service life of reinforced concrete (RC) structures exposed to aggressive environments. This corrosion deterioration can lead to damage resulting in capacity loss or even failure. For structures exposed to coastal marine environments or deicing or anti-icing applications, this deterioration is often accelerated.

Over half of the total bridges (604,191 bridges reported by the Federal Highway Administration in 2010) in the US are RC and a study in 2002 indicated that the annual direct cost of corrosion to bridges was \$5.9 to \$9.7 billion (Koch et al. 2002). Based on data from the National Bridge Inventory in 2010, the average bridge age in the country is 40 years old. Thirty percent of the bridges have exceeded 50 years, 7% have exceeded 75 years, and 25% are deemed deficient (structurally deficient or functionally obsolete). For bridges located in coastal areas or exposed to deicing or anti-icing chemicals, these older bridges often experience corrosion of the reinforcement due to high chloride concentrations. When reinforcement corrodes, the integrity and likely the capacity of the structure is reduced. In seismic areas, this reduction in capacity may be magnified due to the loading demands during a seismic event. Therefore, understanding the time-variant risks associated with corroding structures will assist engineers and decision makers in making sound decisions with respect to optimization of design, inspection, repair, strengthening, and/or replacement of RC structures.

The corrosion deterioration in RC structures has raised significant attention from researchers and analytical and experimental studies have been performed worldwide. Durability and serviceability of corroded RC structures have been investigated to determine the relationship between the corrosion process and the service life of these structures and these relationships have been used to develop service life models. The American Association of State Highway and Transportation Officials (AASHTO) offers standard procedures for the design of highway bridges but does not provide clear guidance on predicting the long-term effects of reinforcement corrosion and the long-term reliability of the system. Corrosion of the reinforcement could be especially

detrimental to the seismic performance of bridge structures and limited efforts have been made to model the structural performance of RC structures exhibiting corrosion during seismic events. The objective of this paper is to first develop a realistic corrosion rate model that represents actual corrosion conditions and then, using this model, develop another model to predict the time-variant seismic performance of RC bridge columns exhibiting corrosion of the steel reinforcement. This information can then be used to optimize design, maintenance, repair, strengthening, and/or replacement of RC bridges.

The service life of RC structures subject to corrosion is comprised of two general phases: the initiation and the propagation phases. Initiation is the depassivation process of reinforcement, where the aggressive agents are transported into the concrete to the steel reinforcement surface. Propagation begins when the steel is depassivated, causing active corrosion, and terminates when the RC structure reaches the end of its service life. Because cracking affects serviceability, most papers further divide the corrosion propagation phase into two sub-phases: the first sub-phase is the pre-cracking phase and the latter sub-phase is the post-cracking phase which is also referred to as the deterioration phase. Figure 1 shows structure damage versus time and shows the phases and sub-phases. Because significant work has been performed on the initiation phase, this paper will focus on the propagation phase of the deterioration process.

Significant efforts have been made in modeling the initiation phase. Much less efforts have focused on the propagation phase. Different prediction models have been developed to simulate the corrosion process, including empirical models, numerical models (finite element method, boundary element method, and resistor networks and transmission line approach), and analytical models (Otieno et al. 2011). This study provides a critical review of existing models used to predict the corrosion propagation of steel in RC structures. This review is followed by the development of a new model that incorporates critical parameters for modeling the corrosion propagation phase. The new model is based on the physical process and is calibrated with a set of measured long-term field data. This new model is then used to predict corrosion deterioration of a RC column. The column is then analyzed for seismic performance. A reliability analysis of the lateral capacity of the column is then performed. The example column is for a typical highway bridge built in Oregon in the early 1970s.
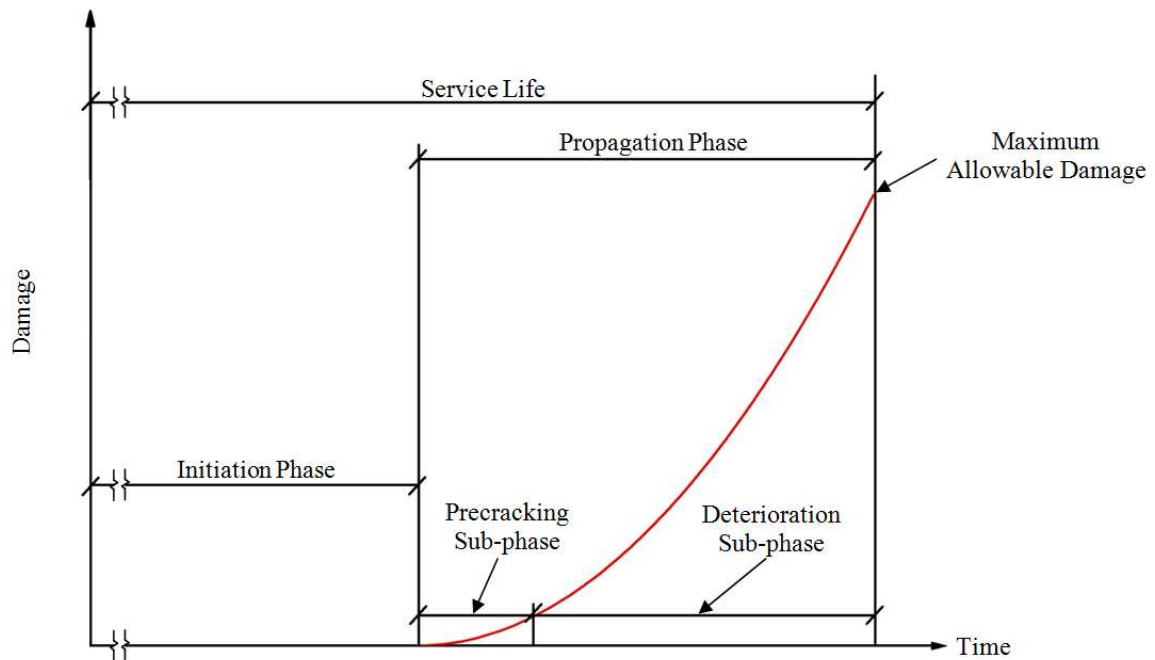
Figure 1. Different phases of service life for a corroding structure

MODELING CORROSION: INITIATION AND PROPAGATION PHASES

ASTM terminology defines corrosion as "the chemical or electrochemical reaction between a material, usually a metal, and its environment that produces a deterioration of the material and its properties" (ASTM G193). During the electrochemical process, iron is oxidized to iron ions to form corrosion products. The oxidation of iron has two consequences: a reduction in the cross section of the steel reinforcement and the formation of corrosion products of increased volume, which results in cracking and spalling of the concrete cover. Reduced steel cross sections can result in reduced capacity and loss of concrete cover can result in reduced stiffness. The following sections provide an overview of the initiation and propagation phases.

Initiation Phase

The time from when a structure is placed into service to the time when the steel depassivates is defined as the initiation phase. Steel reinforcement in RC structures is usually well protected unless aggressive elements are transported to the steel surface and destroy the protective passive layer. The ingress of chloride ions (Cl⁻) and/or carbon dioxide (CO_2) are the main causes of corrosion initiation and propagation. The four basic mechanisms of transport of these aggressive ions include capillary suction, permeation, diffusion, and migration. The duration of the initiation phase depends principally on the transport rate of the aggressive elements, the environmental conditions, and design parameters (mainly cover).

This paper focuses on chloride-induced corrosion. The primary mechanism for chloride transport through the concrete pore system is diffusion. To predict the time to corrosion (i.e. the duration of the initiation phase), many models have been developed, including STADIUM, Life-365, ConcreteWorks, and DuraCrete. STADIUM uses time-step finite element analysis to simulate the transportation of chlorides through concrete, considering the concrete properties. Life-365, ConcreteWorks, and DuraCrete are all based on Fick's second law for chloride concentration prediction and corrosion initiation. In chloride-induced corrosion models, the solution for infinite-source diffusion of chlorides at depth x and time t can be estimated using Fick's second law:

$$C(x,t) = C_s \left[1 - erf \left(\frac{x}{2\sqrt{D_a t}} \right) \right] \tag{1}$$

where C_s is the chloride concentration on the concrete surface, D_a is apparent diffusion coefficient (length^2/time), t is time, and x is the distance from any point inside the concrete to the surface (length). Life-365, ConcreteWorks, and DuraCrete use modified models and input variables such as chloride exposure conditions, of environmental temperatures, concrete mixture proportions, surface barrier types, and curing conditions. When the chloride concentration at the reinforcement surface reaches a critical value (termed the critical chloride concentration), the reinforcing steel depassivates and corrosion initiates.

Propagation Phase: Corrosion Rate Models

Significant work has been performed to determine the duration of the initiation phase for the service life of RC structures. The science and engineering communities use these models to predict the duration of the initiation phase. Fewer models are available to determine the duration of the propagation phase. Corrosion results in the formation of corrosion products ($Fe(OH)_2$ and $Fe(OH)_3$ are dominant products) which have been reported to be 4 to 6 times the volume of the metal iron (Bertolini et al. 2004). Continued corrosion reactions result in corrosion products filling the concrete pores around the reinforcing steel. With time, the continued formation of corrosion products results in internal stresses in the concrete, which causes cracking of the concrete cover and eventual spalling.

During the propagation phase, the corrosion rate is an important factor for assessing the duration of the propagation phase and the damage resulting from the corrosion. Therefore, corrosion rate models have been developed, most of them empirical, estimating corrosion rate as a function of time. Most analyses assume that the corrosion rate is constant during the service life (Alonso et al. 1988; Andrade et al. 1993; Stewart and Rosowsky 1998; Ahmad and Bhattacharjee 2000; Martinez and Andrade 2009). Other researchers assumed time variant models (Yalçyn and Ergun 1996; DuraCrete 2000; Vu and Stewart 2000; Li 2004). These models are shown in Table 1 and plotted in Figure 2. The values in Figure 1 assume a water-cement ratio of 0.45 and a cover depth of 51 mm (2 in.). The seemingly apparent drawback of these models is that they do not represent the actual corrosion conditions of a corroding system. Trejo and Monteiro (2005) reported that the corrosion rate increases from 0 (or a very low value) prior to initiation to a maximum value at a relatively early age and then decreases to a near constant value. Vu and Stewart (2000) postulated that this decrease may be a result of the reduction in the anode to cathode area ratio and the formation of the corrosion products on the steel surface. The model by Ahmad and Bhattacharjee (2000) considers several parameters that influence the corrosion rate, but such constant corrosion rate models are not representative of actual corrosion rates. In addition, Vu and Stewart's model does not consider temperature, which can significantly affect the corrosion rate. Furthermore in the model by Vu and Stewart (2000), the corrosion rate is infinity at time zero, which is not realistic. Li's (2004) model does not consider potential influencing parameters, including concrete characteristics and environmental conditions. In addition, the corrosion rate continuously increases with time, which does not correlate with reported data in the literature

(Liu and Weyers 1998; Trejo and Monteiro 2005). The magnitude of corrosion rate could significantly alter the duration of the propagation phase and inaccurate corrosion rates could result in inaccurate estimates of the time-variant damage.

An appropriate model to determine the duration of the propagation phase must be based on a reasonable corrosion rate model and should correlate with data from long-term tests. In this paper, existing models are compared with results from long-term data from the literature. Liu and Weyers (1998) reported the corrosion performance of 44 RC slabs over a 5 year period when subjected to severe exposure conditions (Figure 2). Five outdoor specimens contained no admixed chloride, a water-to-cement ratio was 0.45, and the cover depth was 51 mm (2 in.). The specimens were exposed to corrosion environment. Figure 3 shows the corrosion rate data after corrosion propagation collected from the experiments. Liu and Weyers (1998) reported that the corrosion rate in concrete, $i_{\mathrm{corr}}(t)$, is a function of concrete temperature, ohmic resistance, chloride concentration, and exposure time as follows:

$$i_{\mathrm{corr}}(t) = 0.9259 e^{\left[8.37 + 0.618 \ln(1.69 Cl) - \frac{3034}{T} - 0.000105 R_c + 2.32 t^{-0.215} \right]}$$
(2)

where $i_{\mathrm{corr}}(t)$ is the corrosion current density (μA/cm^2), Cl is chloride concentration (kg/m^3), T is the annual mean concrete temperature at the depth of the steel surface (degree K), R_c is the ohmic resistance of the concrete cover (ohms), and t is the time (yr) after corrosion initiation. This model results in a decreasing corrosion rate with increasing time but results in an infinite corrosion rate at time zero. In addition, the model does not reflect seasonal temperature changes that occur throughout the year.

To objectively assess the models documented in the literature, a comparison of models reported in the literature will be performed with the data from Liu and Weyers (1998). The amount of current passed (coulombs) of each model will be compared with the coulombs passed reported in Liu and Weyers (1998). The unit coulombs passed will be used to make the comparison and is defined here as the charge passed as a result of the corrosion process per unit area (cm^2) over a defined time period. The units of a unit coulomb is A·sec/cm^2.

The shaded areas in Figure 3 represent the unit coulombs passed from the data reported by Liu and Weyers (1998). Every year is divided into 12 increments. When data are not available, linear interpolation between the two closest mean values was used to estimate the mean value of the

corrosion rate. The area of a shaded column represents the unit coulombs passed in that month. The calculated unit coulombs passed from each corrosion rate model is then compared with this long-term data from Liu and Weyers (1998). The percent errors of each model can then be determined and plotted. Figure 4 shows the percent error for each model calculated as follows:

$$\% \text{ error} = \frac{\text{unit coulombs passed from model - unit coulombs passed from experiments}}{\text{unit coulombs passed from experiments}} \times 100$$

(3)

To estimate the long-term corrosion activity from Liu and Weyers' data (i.e., from year 5 to 10), it was assumed that corrosion rate data for years 3 and 4 are representative of corrosion rates for years 5 to 10. For the 5th year, Liu and Weyers only show data for 9 months but the unit coulombs passed for the 4th and 5th year for the same 9-month period are very similar. Therefore, the unit coulombs passed after the 4th year is considered constant for every year after the 4th year.

Among the models shown in Figure 5, Vu and Stewart's model significantly underestimates the corrosion rate. Li's model and Yalcyn and Ergun's model initially underestimate the corrosion rate but overestimate the corrosion rate later. Liu and Weyer's model initially overestimate the corrosion rate but underestimate the corrosion rate later. The other models consistently overestimate the corrosion rate. Underestimation of the corrosion rate could lead to overestimation of the service life, unexpected damage or failure, and decreased safety. In addition, overestimation of the corrosion rate could lead to underestimation of the service life, improper cost analysis, and improper planning.

Because the corrosion rate is a critical factor for predicting the effect of corrosion in RC structures, improving the accuracy of the corrosion rate could improve the accuracy of the prediction models for assessing service life of RC structures. Challenges with existing corrosion rate models show the need for the development of a new model. The following section provides justification for a new model.

Table 1. Existing corrosion rate models

Author(s)	Type	Model	Input variables
Stewart and Rosowsky (1998)	Constant	$i_{corr} = 1.5 \ [\mu A / cm^2]$	NA
Alonso et al. (1988)	Constant	$i_{corr} = \dfrac{1000}{\rho_{con}} \ [mA / m^2]$	ρ_{con} is concrete resistivity.
Martinez and Andrade (2009)	Constant	$i_{corr} = B / R_p \ [\mu A / cm^2]$	B is a constant resulting from a combination of the anodic and cathodic Tafel slopes, R_p is the polarization resistance in kΩ cm^2.
Ahmad and Bhattacharjee (2000)	Constant	$i_{corr} = 37.726 + 6.12 \cdot C \cdot 2.231 \cdot A^2 \cdot B + 2.722 \cdot B^2 \cdot C^2 \ [nA / cm^2]$	$A = \dfrac{\text{Cement Content (kg/m}^3\text{)} - 300}{50}$, $B = \dfrac{w/c - 0.65}{0.075}$, $C = \dfrac{\%CaCl_2 \text{(by weight of cement)} - 2.5}{1.25}$.
DuraCrete (2000)	Exponential decrease	$i_{corr}(t) = \dfrac{k_0}{\rho(t)} \cdot F_{Cl} \cdot F_{Galv} \cdot F_{Oxide} \cdot F_{O_2} [\mu A / cm^2]$ where $\rho(t) = \rho_0 \cdot f_e \cdot f_t \cdot \left(\dfrac{t}{t_0}\right)^n$	k_0 is a constant regression parameter (10^4) F_{Cl} is a factor which takes account of the influence of the chloride content, F_{Galv} is a factor which takes account of the influence of galvanic effects, F_{Oxide} is a factor which considers the influence of continuous formation of oxides and ageing upon the corrosion rate, $\rho(t)$ is the actual resistivity of concrete measured by a compliance test, in [Ωm] at time t, ρ_0 is the resistivity of the concrete measured by a compliance test, in [Ωm] at time t_0 n is a factor which takes account of the influence of ageing on ρ_0, f_e is a factor which modifies ρ_0 to take account of the influence of the exposure, f_t is a factor which takes into account the influence of the resistivity test method.
Yalçyn and Ergun (1996)	Exponential decrease	$i_{corr}(t) = i_{corr,0} \cdot e^{(-1.1 \times 10^{-3} t)} \ [\mu A / cm^2]$ where $i_{corr,0} = 0.53 \ \mu A/cm^2$	t is time (day) from corrosion initiation
Vu and Stewart (2000)	Exponential decrease	$i_{corr}(t) = i_{corr,0} \cdot 0.85 \cdot t^{-0.29} \ [\mu A / cm^2]$ * where $i_{corr,0} = \dfrac{37.8(1 - w/c)^{-1.64}}{d_c}$	w/c is the water-to-cement ratio, d_c is the concrete cover depth (mm).
Li (2004)	Logarithmic increase	$i_{corr}(t) = 0.3683 \cdot \ln(t) + 1.1305 \ [\mu A / cm^2]$	t is time (yr) from corrosion initiation

* For typical environmental condition (the ambient relative humidity of 75% and a temperature of 20°C).
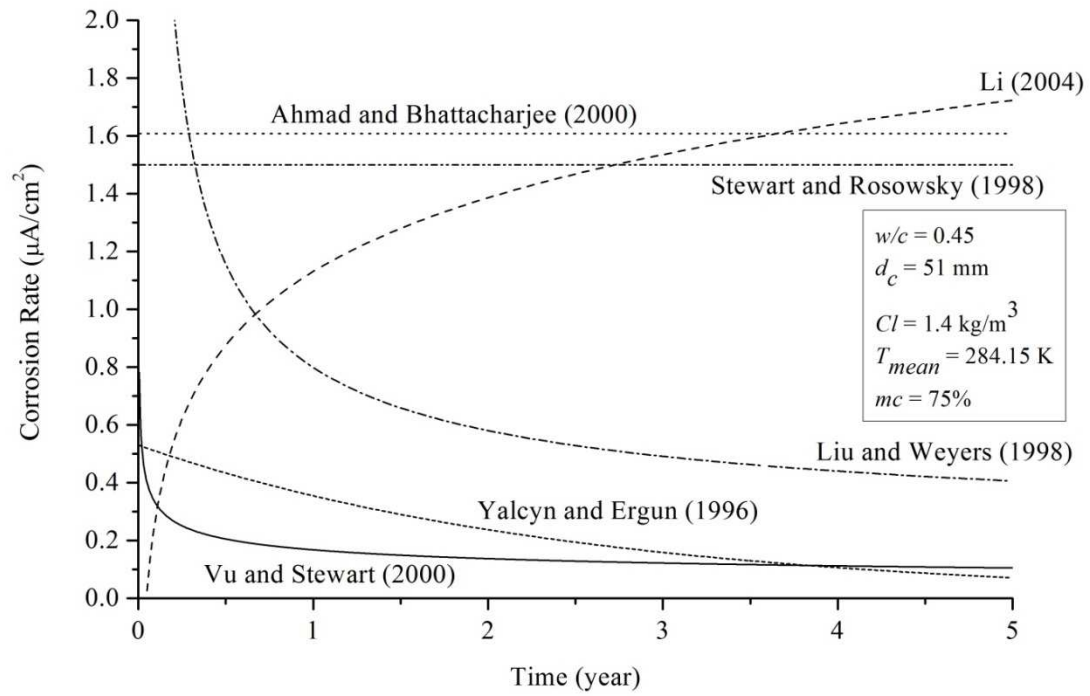
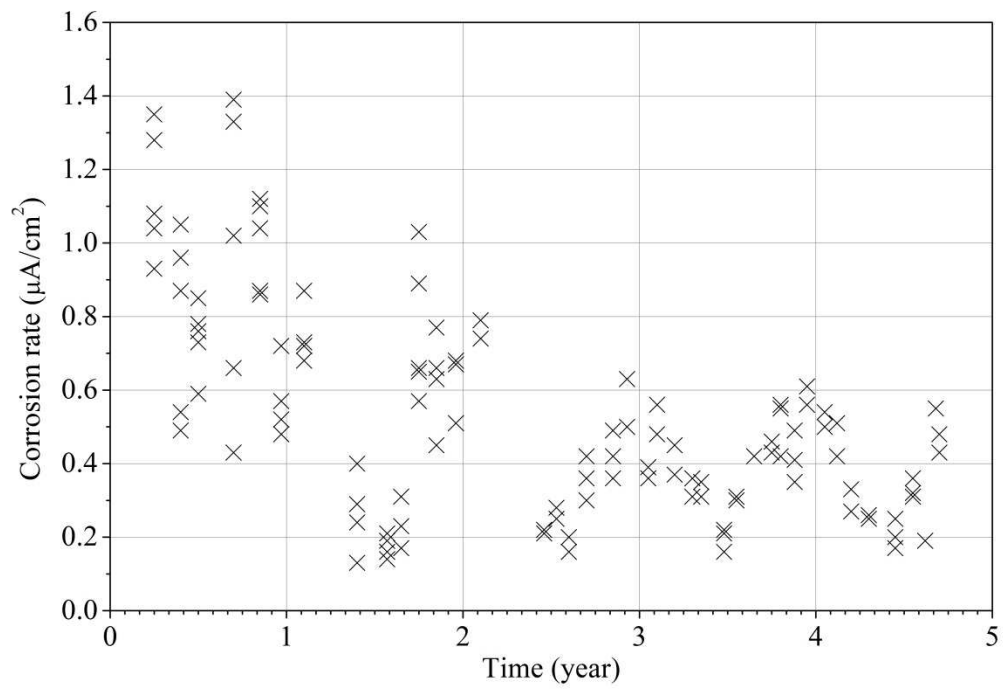Figure 2. Plots of different corrosion rate models

Figure 3. Corrosion rate data reported by Liu and Weyers (1998)
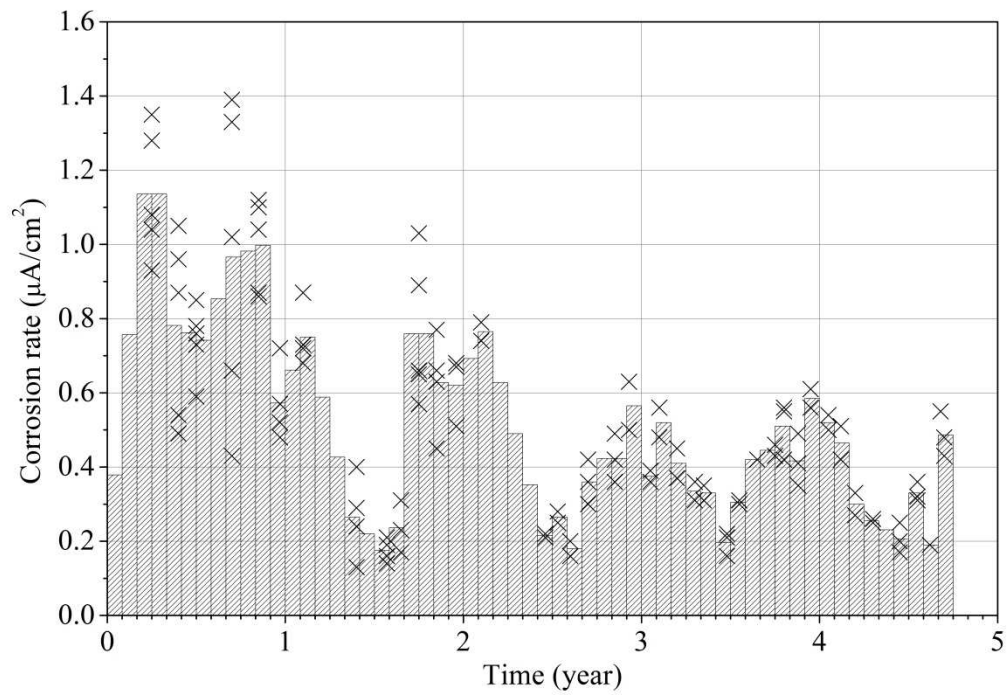
Figure 4. Unit coulombs passed from the data reported by Liu and Weyers (1998)
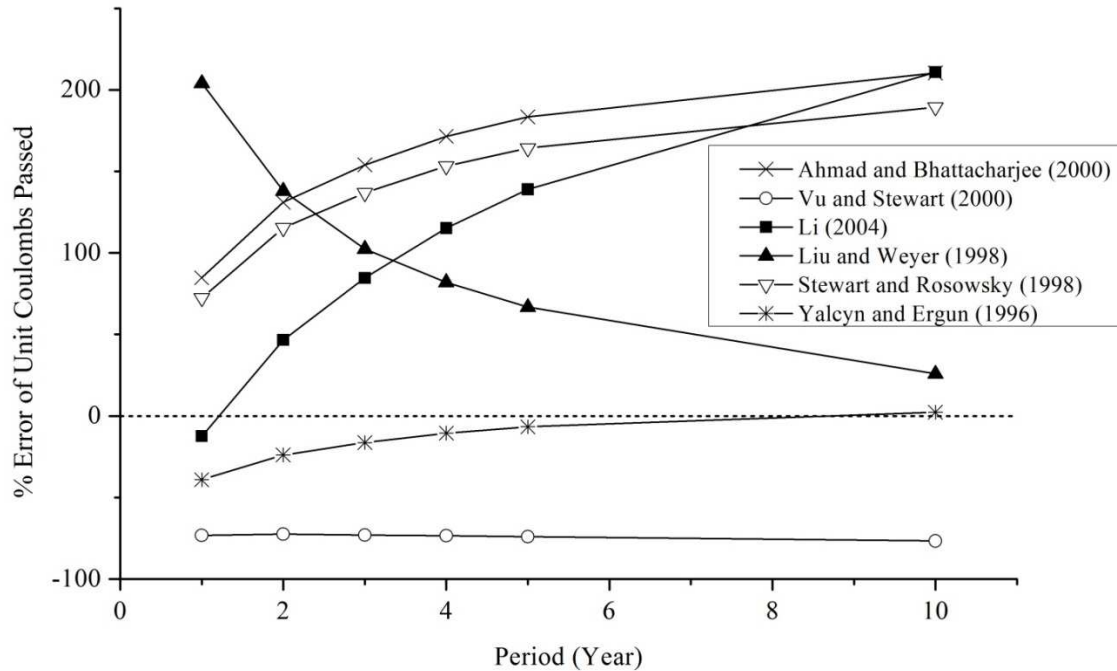
Figure 5. Percent error of unit coulombs passed for different models
compared to data reported by Liu and Weyers (1998)

DEVELOPMENT OF A NEW MODEL FOR ESTIMATING THE DURATION OF THE PROPAGATION PHASE

The corrosion of steel in concrete is a complex electrochemical process and the literature shows that the corrosion rate is strongly affected by the concrete characteristics and the environmental conditions. As with all electrochemical cells, the resistivity of the electrolyte, the oxygen concentration, and the availability of moisture influence the corrosion rate. For RC systems, the electrolyte resistivity is dependent on the concrete characteristics. The water-to-cement ratio (or water-to-cementitious materials ratio), moisture content within the concrete pores, temperature, chloride concentration, and in some cases the concrete cover are factors that influence the electrolyte resistivity. Figure 6 shows the relationships between these factors. A reasonable corrosion rate model should be a function of the concrete characteristics and the environment in

which the concrete is placed. A general expression of the corrosion rate function can be expressed as:

$$i_{corr}(t) = i_{corr,0} \cdot f_{O_2} \cdot f_{mc} \cdot f_{res} \cdot f_{Cl} \cdot f_{w/c} \cdot f_{d_c} \cdot f_T \tag{4}$$

where f_{O_2}, f_{mc}, f_{res}, $f_{w/c}$, f_{d_c}, f_T, and f_{Cl} are factors that consider the influence of oxygen concentration, moisture content, concrete resistivity, water-to-cement ratio, concrete cover depth, temperature, and chloride concentration, respectively, and $i_{corr,0}$ is the basic corrosion rate. The effect of these factors will be presented in the following paragraphs. Note that the environmental factors for this model represent the conditions at the reinforcing steel surface and that ambient conditions influence these conditions at the steel surface. Liu and Weyers (1998) and Trejo and Monteiro (2005) reported that the corrosion rate increases from 0 (or a very low value) prior to corrosion initiation to a maximum value at a relatively early age and then decreases. These changes in corrosion rate are dependent on the local conditions at the steel-concrete interface.

Oxygen and moisture are necessary for most electrochemical reactions to occur. Although the oxygen concentration in air for a certain location is nearly constant, the concentration at the steel-concrete interface can be different and may vary with time. The oxygen concentration at the steel surface is mainly determined by the access of air to the concrete surface and the transportation of oxygen through the concrete pores. The oxygen diffusion coefficient is found to increase with increasing *w/c*, increase with decreasing salt content, increase with increasing temperature, and increase with decreasing moisture content (Kobayashi and Shuttoh 1991; Ahmad 2003; Böhni 2005). Among all these influencing factors, the moisture content in the concrete pores has a dominating influence on the oxygen concentration at the steel surface. When the moisture content in the concrete pores is high, the diffusion rate of oxygen is very low because the diffusion coefficient of oxygen in the water is much lower than the diffusion coefficient of oxygen in air (Balabanic et al. 1996; Böhni 2005). The moisture content depends mostly on the exposure conditions (Bertolini et al. 2004). Experiments have shown that the corrosion rate is very low when the moisture content in the concrete pores is less than 50%, increases exponentially when the moisture content raises to 50% to 70%, remains nearly constant from 70% to 90%, and then decreases when the moisture content is above 90% (Balafas and Burgoyne 2010). The last decrease is a result of the lack of oxygen availability. Using the experimental data reported by Balafas and Burgoyne (2010), the moisture factor, f_{mc}, can be estimated as:

$$f_{mc} = e^{-6000(mc-0.75)^6} \tag{5}$$

where *mc* is the moisture content in percent divided by 100. The values of f_{mc} as a function of concrete moisture content are shown in Figure 7. This indicates that corrosion rate will be maximum in the range from 70% to 90% and is reduced when outside of this range.

In addition to oxygen and moisture, the electrical resistivity of concrete also has a significant effect on the corrosion of reinforcing steels in concrete. Alonso et al. (1988) and Lopez and Gonzalez (1993) reported that concrete resistivity and corrosion rate are inversely proportional over a wide range of concrete resistivity values. The literature also shows that concrete resistivity is strongly affected by the concrete characteristics, the degree of concrete pore saturation, and the chloride concentration (Hussain et al. 1995; Morris et al. 2004; Song and Saraswathy 2007). Low resistivity values are associated with high water-to-cement ratio values, high chloride concentrations, and/or high moisture contents (Neville 1996; Morris et al. 2004). Because the resistivity is strongly influenced by the chloride concentration, moisture content, and *w/c*, modeling the corrosion rate during the propagation phase can include either resistivity or these three variables (chloride concentration, moisture content, and *w/c*), but likely not both. This model will include concrete moisture content, chloride concentration, and *w/c* and not the resistivity of the concrete.

Experiments have shown that the corrosion rate increases as the chloride concentration increases in concrete (Liu and Weyers 1998). It has been reported that one reason for this increase is the increase in the conductivity of the concrete as the chlorides increase. Another reason is that chlorides act as a catalyst for the corrosion process, accelerating the electrochemical reactions. Because the chloride threshold has already been reached (this model is for the corrosion propagation phase only), the main effect of chlorides is to change the resistivity of the concrete. Because the chloride concentration is higher than the chloride threshold during the propagation phase, the chloride factor, f_{Cl}, can be expressed using the chloride concentration of the concrete and the chloride threshold of the steel reinforcement. Based on the relationship between corrosion rate and chloride concentration reported by Liu and Weyers (1998), the chloride factor can be estimated as follows:

$$f_{Cl} = \frac{Cl + Cl_{Th}}{2Cl_{Th}} \qquad (6)$$

where Cl is the water soluble chloride concentration at the steel surface (kg/m^3 or lb/ft^3) and Cl_{Th} is the chloride threshold of the steel reinforcement required for corrosion initiation (kg/m^3 or lb/ft^3).

It has been reported in the literature that w/c and concrete cover depth also significantly affect the corrosion rate. The pore size distribution and the transport properties of concrete are direct functions of w/c. The resistivity of uncontaminated concrete is also mainly controlled by w/c. The time for water, oxygen, and chlorides to be transported through the concrete to the steel interface are directly related to concrete cover depth as well as the w/c (Bertolini et al. 2004). Therefore, w/c and concrete cover depth are important variables influencing the corrosion rate. Vu and Stewart (2000) and Bertolini et al. (2004) reported that the corrosion rate is inversely proportional to concrete cover depth and directly proportional to w/c. As already noted, the corrosion rate model developed by Vu and Stewart (2000) underestimates the corrosion rate. However, as shown in Figure 5, the model shows a near constant error when compared with the data from Liu and Weyers (1998). This indicates that the relationship between the concrete characteristics (w/c and d_c) and the corrosion rate is likely valid. As such, the term for the concrete characteristics in the Vu and Stewart (2000) model will be used here to include the effect of w/c and concrete cover depth on the corrosion rate, and f_{conc} will be defined as:

$$f_{conc} = k_c \frac{(1 - w/c)^{-1.64}}{d_c} \qquad (7)$$

where k_c is a constant and d_c is the concrete cover depth (mm or in.).

In addition to concrete characteristics, temperature influences the corrosion rate. In RC systems, the temperature affects the mobility of ions and solubility of salts, affects the degree of the concrete pore saturation, and thus influences the rate at which the electrochemical reactions occur (Lopez and Gonzalez 1993; Broomfield 1997). For reinforcing steels embedded in concrete, the effect of temperature is complex. The corrosion rate increases with increased temperature, however, the solubility of oxygen in the pore solution decreases with increasing temperature, and the two effects offset each other (Jones 1996). Work by Pour- Ghaz et al. (2009) showed that the

effect of temperature on the corrosion rate for common exposure conditions (from 280 K to 330 K) could be estimated using the Arrhenius equation. Therefore, the annual mean temperature factor, $f_{T_{mean}}$, can be defined as:

$$f_{T_{mean}} = e^{2283\left(\frac{1}{284.15} - \frac{1}{T_{mean}}\right)} \tag{8}$$

where T_{mean} is the annual mean temperature at the depth of steel surface (degree K).

In addition to the annual mean temperature, seasonal temperature fluctuation also can influence the corrosion activity and should be considered in estimating the corrosion rate, especially at early ages of corrosion. As reported by Liu and Weyers (1998), the corrosion rates are highest in mid-summer (during the highest average temperatures) and lowest in mid-winter (during the lowest average temperatures). A periodic function can be used to represent changes in corrosion rate as a function of seasonal temperature changes. A sine function with a one-year period could be a good model to represent this seasonal temperature effect. The annual mean, average high, and average low temperatures, all of which are readily available on the internet (e.g. the database of National Oceanic and Atmospheric Administration), can then be used to determine corrosion rates.

Liu and Weyers (1998) considered several influencing factors affecting corrosion rate and developed the corrosion rate model shown in Equation (2). This model provided significant advances for modeling the corrosion rate in the propagation phase for RC systems. However, this model does not include some key influencing factors. Therefore, a new corrosion rate model based on the data measured from the long-term tests by Liu and Weyers (1998) that includes the influencing factors discussed (moisture content, chloride content, w/c, concrete cover depth, annual mean temperature, and seasonal temperature changes) is proposed. For conventional reinforcing steels, the corrosion current density $i_{corr}(t)$ in μA/cm^2 can be expressed as a function of time, t (yr), using the relationships as follows:

$$i_{corr}(t) = i_{corr,0} \cdot f_{mc} \cdot f_{Cl} \cdot f_{conc} \cdot f_{T_{mean}} \cdot f_{T_{seasonal}} \tag{9}$$

where f_{mc}, f_{Cl}, f_{conc}, $f_{T_{mean}}$, and $f_{T_{seasonal}}$ are factors that take into account the influence of the moisture content, the chloride concentration, the concrete characteristics (water-to-cement ratio

and the concrete cover depth), the annual mean temperature, and the seasonal temperature changes. The factors f_{mc}, f_{Cl}, f_{conc}, and $f_{T_{mean}}$ are defined in Equations (5), (6), (7), and (8) respectively. A reciprocal function is used here to show the continuous decrease in corrosion rate and a sine function is used to show the effect of cyclic seasonal temperature changes. The reciprocal function and the sine function are combined by best fitting the data reported by Liu and Weyers (1998), and the combined function is:

$$f_{T_{seasonal}} = \frac{k_1 \sin(t)}{t} + k_2 \tag{10}$$

where k_1 and k_2 are influencing parameters determined from data fitting and t is time (year). Including the effect of average high temperature, average low temperature, and the time when corrosion initiates, Equation (10) can be written as:

$$f_{T_{seasonal}} = \frac{(T_{high} - T_{low}) \sin(2\pi(t - a_s))}{8.6(t - a_s)} + 7.6 \tag{11}$$

where T_{high} is the average high temperature (K), T_{low} is the average low temperature (K), and a_s is the corrosion initiation season factor which is 0.07, 0.7, 0.43, and 0.25 for spring, summer, fall, and winter respectively. The constants 8.6 and 7.6 are determined by moving and stretching the function to best fit the measured data and 2π is used to adjust the period of the sine function to 1 year. By substituting all the factors into Equation (9), the complete expression of the new corrosion rate model is:

$$i_{corr}(t) = \underbrace{\left[e^{-6000(mc-0.75)^6} \right]}_{\text{moisture content}} \cdot \underbrace{\left(\frac{Cl + Cl_{Th}}{2Cl_{Th}} \right)}_{\text{chloride concentration}} \cdot \underbrace{\left[\frac{(1 - w/c)^{-1.64}}{d_c} \right]}_{\text{concrete charactoristics}} \cdot \underbrace{\left[e^{2283\left(\frac{1}{284.15} - \frac{1}{T_{mean}} \right)} \right]}_{\text{annual mean temperature}} \cdot \underbrace{\left[\frac{(T_{high} - T_{low}) \sin(2\pi(t - a_s))}{8.6(t - a_s)} + 7.6 \right]}_{\text{seasonal temperature}}$$

$$\tag{12}$$

Figure 8 shows the prediction of the corrosion rate using the proposed model. Rearranging the terms in the corrosion rate model in Equation (12), this model can be more simply expressed as:

$$i_{\text{corr}}(t) = \frac{(1-w/c)^{-1.64}}{d_c}\left(\frac{Cl+Cl_{Th}}{2Cl_{Th}}\right)\left[\frac{(T_{high}-T_{low})\sin(2\pi(t-a_s))}{8.6(t-a_s)}+7.6\right]e^{2283\left(\frac{1}{284.15}-\frac{1}{T_{mean}}\right)-6000(mc-0.75)^6}$$

(13)

For this model, the corrosion rate first increases from a low value to a maximum value at a relatively early age and then decreases as reported by Liu and Weyers (1998) and Trejo and Monteiro (2005). The corrosion rate then oscillates around a near constant value with a one-year frequency and this oscillation is dependent on the difference in the seasonal temperatures. The percent error of the coulombs passed of proposed model compared with data reported by Liu and Weyers (1998) is zero at the early age and then increases to a constant value of 5% after the second year.

A sensitivity analysis is performed to determine which variables in the corrosion rate model are most sensitive. Figure 9 shows the result of the sensitivity analysis. The results show that the corrosion rate is most sensitive to the annual mean temperature. The corrosion rate is also sensitive to lower and higher moisture contents, high *w/c*, and low concrete cover.

Using known influencing variables, the proposed corrosion rate model is more representative of actual corrosion than existing models. The evaluation of the effect of corrosion on RC structures includes the assessment of the residual load-carrying capacity of existing structures and the prediction of structural performance and service life of new structures. Therefore, a more representative corrosion rate model will assist engineers and decision makers in making better decisions regarding designing, inspection, repair, strengthening, and/or replacement of RC structures.
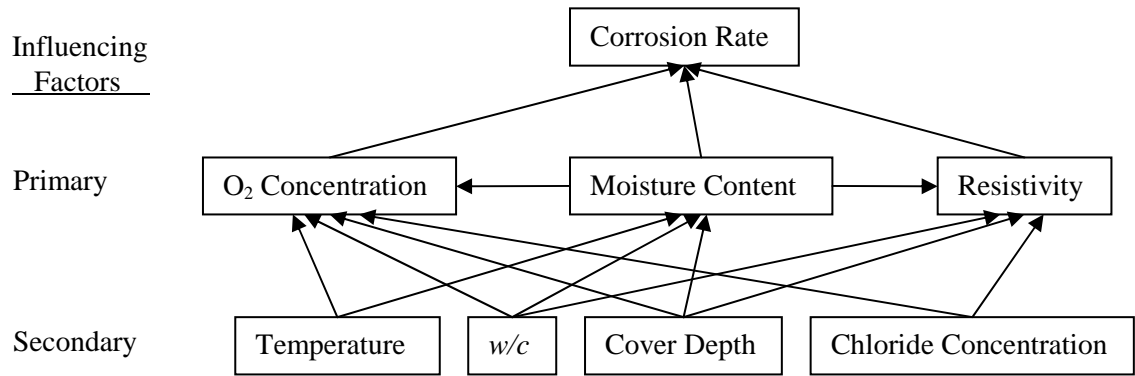
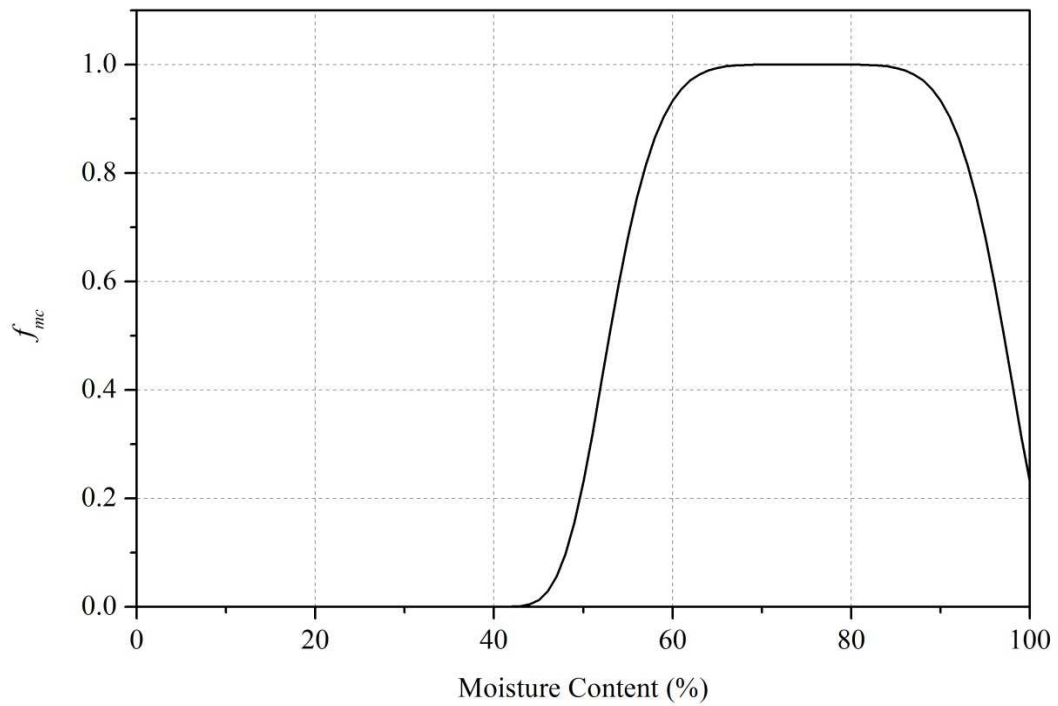Figure 6. Primary and secondary factors influencing corrosion rate

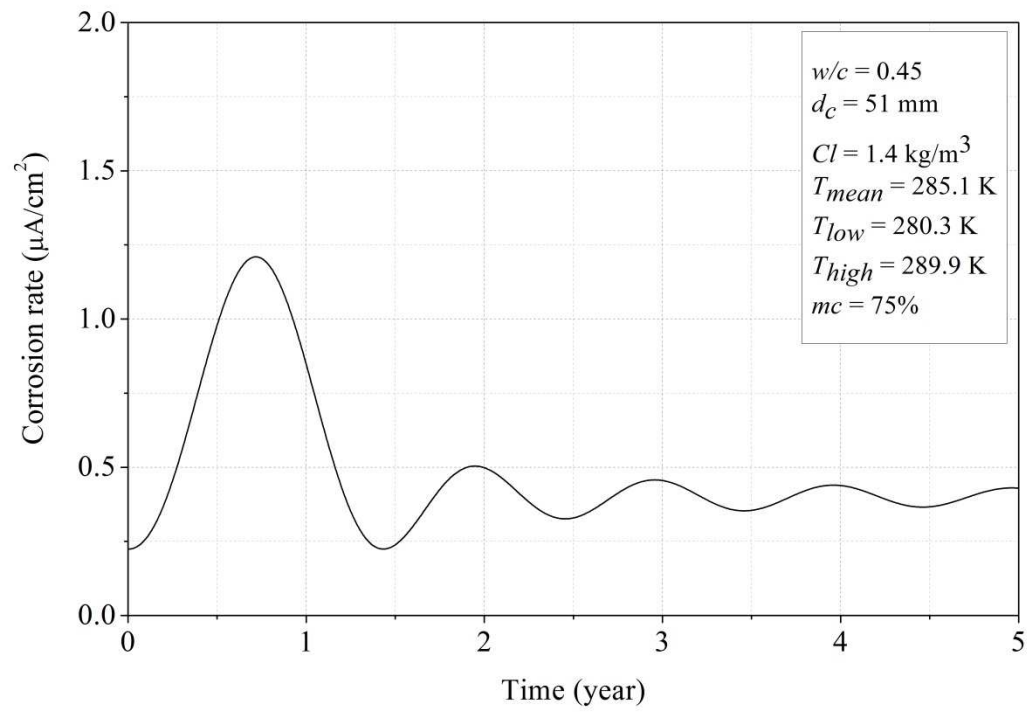Figure 7. Moisture content factor influencing corrosion rate

Figure 8. New proposed corrosion rate model
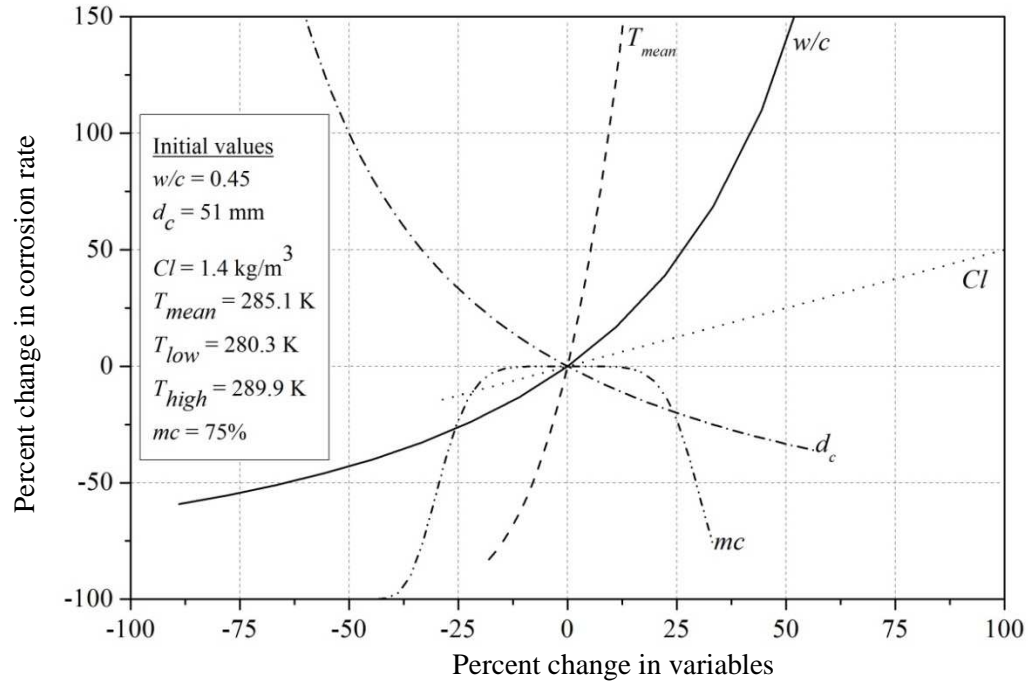
Figure 9. Sensitivity of corrosion rate to variables

MODELING CORROSION EFFECTS ON LATERAL PERFORMANCE OF BRIDGE COLUMNS

Corrosion of reinforcement can be especially detrimental to the performance of bridge structures. The corrosion rate is an important factor to assess damage resulting from the corrosion. The proposed corrosion rate model can be used to model the corrosion deterioration of bridge structures and members. In this study, the lateral capacity loss of a bridge column will be evaluated using the proposed corrosion rate model.

Prediction of lateral capacity loss of bridge columns under corrosion attack can be estimated using: 1) strength loss resulting from the decrease of steel area; 2) loss of bond between concrete and reinforcement; and 3) stiffness degradation resulting from loss of concrete cover. The bond loss and stiffness degradation are a result of the expansive corrosion products (rust) that cause

internal microcracking, external longitudinal cracking, and eventually spalling. The effect of bond loss is not considered in this paper, because it has been reported that the reduction of bond has a negligible effect on bridge reliability in flexure for typical corrosion rates (Vu and Stewart 2000). This is also supported by other experimental results (Fang et al. 2004; Wang and Liu 2004), which show that the pullout resistance of RC members with confinement (i.e. stirrups) is not significantly affected by corrosion. In addition, because the bridge column example in this paper has a high transverse steel ratio to confine the core concrete, the effect of bond loss would be expected to be minimal.

Choe et al. (2009) and Simon et al. (2010) reported that small reductions in the area of the longitudinal reinforcement in a column and footing caused by corrosion may not have a significant effect on the seismic performance. However, further loss of the reinforcement's cross-sectional area (probably more than 10%) and spalling of concrete cover could affect the lateral strength and stiffness of RC structures. The following section will provide background on the effects of decreasing reinforcement diameter and concrete cover integrity.

Diameter Decrease of Reinforcing Steel

This study will assume that corrosion is generally uniform over the reinforcing steel surface. For the assumed uniform corrosion, the diameter of the reinforcing bars will decrease with time and corrosion rate, and the reduced diameter can be estimated using Faraday's Law as:

$$D(t) = D_0 - k_{corr} \int_0^t i_{corr}(t)\, dt \tag{14}$$

where $D(t)$ is the reduced diameter (length) of the reinforcing bar at some time, D_0 is the initial diameter of the reinforcing bar (length), $i_{corr}(t)$ is the corrosion rate (current/area^2), t is the time from corrosion initiation, and k_{corr} is the corrosion rate conversion factor which is 0.023 to convert corrosion rate from $\mu A/cm^2$ to mm/year.

Stiffness Degradation of Concrete Cover Resulting from Reinforcement Corrosion

During the corrosion propagation phase, significant efforts have been made in developing corrosion-cracking models (Bazant 1979; Alonso et al. 1998; Liu and Weyers 1998; Torres-Acosta and Sagues 2004; Vu et al. 2005). These analytical models use closed-form solutions to model the corrosion process and this approach has been mostly used to model corrosion-induced

cracking. The boundary condition at the concrete-steel interface is assumed to be displaced by expansive corrosion products which result in the evolution of an expansive radial pressure at the boundary. When the stress at the boundary exceeds the tensile capacity of the concrete, the concrete will crack. Li et al. (2006) and Zhong et al. (2010) further developed models using this approach to assess the stiffness degradation of the concrete cover resulting from cracked concrete caused by corrosion of reinforcement.

The concrete with embedded reinforcing bar is commonly modeled as a thick-wall cylinder, as shown in Figure 10(a). In this model, the corrosion-induced cracks are assumed to be smeared and the concrete is considered to be a quasi-brittle material. D_0 is the diameter of reinforcement bar, a and b are the inner and outer radii of the thick-wall cylinder, d_c is the concrete cover depth as defined earlier, r is the distance from any point to the centroid of the cross section of the reinforcing bar, and d_0 is the original thickness of the annular layer of concrete pores prior to corrosion initiation. Once corrosion initiates, a ring of corrosion products forms, as shown in Figure 10(b). The thickness of the corrosion products, $d_s(t)$, can be determined from (Liu and Weyers 1998):

$$d_s(t) = \frac{W_{rust}(t)}{\pi l(D_0 + 2d_0)}\left(\frac{1}{\rho_{rust}} - \frac{\alpha_{rust}}{\rho_{st}}\right) \tag{15}$$

where α_{rust} is a coefficient related to the type of corrosion product, ρ_{rust} is the density of the corrosion products, ρ_{st} is the density of the steel, and l is the unit length (same length units as in ρ_{rust} and ρ_{st}). In this equation, $W_{rust}(t)$ is the mass of corrosion products and is related to the corrosion rate $i_{corr}(t)$ as follows (Liu and Weyers 1998):

$$W_{rust}(t) = 0.81\sqrt{\frac{D_0}{\alpha_{rust}}\int_0^t i_{corr}(t)dt} \tag{16}$$

When the stress at the steel-concrete interface exceeds the tensile strength of the concrete, the concrete will form cracks in the cover. Following Bazant and Planas (1998), the total tangential strain ε_θ after cracking at location r and time t on a surface of the cohesive crack consists of an elastic tangential strain ε_θ^e and an actual cracking strain ε_θ^f as follows:

$$\varepsilon_\theta = \varepsilon_\theta^e + \varepsilon_\theta^f \tag{17}$$

Figure 11(a) shows the stress strain curve of the cracking model. Bazant and Planas (1998) define the stiffness degradation factor, α, as:

$$\alpha = \frac{E_\theta}{E_{ef}} = \frac{\sigma / \varepsilon_\theta}{E_{ef}} \tag{18}$$

where σ is the cohesive stress, E_{ef} is the effective elastic modulus of concrete, and E_θ is the tangential elastic modulus of concrete for unloading. The authors also define the stress-cracking strain relationship (Figure 11(b)) as:

$$\sigma = \varphi(\varepsilon_\theta^f) \tag{19}$$

Li et al. (2006) defined the strain softening curve as:

$$\sigma = \varphi(\varepsilon_\theta^f) = f_t e^{-\lambda \varepsilon_\theta^f} \tag{20}$$

where f_t is the tensile strength of concrete and γ is a material constant. Using this, the stiffness degradation factor, α, can be obtained by substituting Equations (17) and (20) into Equation (18) to get:

$$\alpha = \frac{f_t e^{-\lambda \varepsilon_\theta^f}}{E_{ef} \varepsilon_\theta} = \frac{f_t e^{-\lambda(\varepsilon_\theta - \varepsilon_\theta^e)}}{E_{ef} \varepsilon_\theta} \tag{21}$$

Li et al. (2006) defined the values of ε_θ and ε_θ^e as:

$$\varepsilon_\theta = \frac{(b^{\sqrt{m}} - a^{\sqrt{m}})[c_3(b) + c_4(b)/(ab)^{\sqrt{m}}]}{\sqrt{m}(b-a)} \tag{22}$$

$$\varepsilon_\theta^e = \frac{1}{b-a} \left(\int_a^b c_1(r) + \frac{c_2(r)}{r^2} dr \right) \tag{23}$$

where m is the ratio between the Poisson's ratios in the tangential and radial directions and c_1, c_2, c_3, and c_4 are expressed as:

$$c_1(r) = -\frac{2\sqrt{m}(1-v_c)rd_s(t)}{\Delta}$$

(24)

$$c_2(r) = -\frac{2\sqrt{m}(1+v_c)rb^2d_s(t)}{\Delta}$$

(25)

$$c_3(r) = -\frac{\{(1-v_c)(\sqrt{m}-1)b^2 + [1+v_c + \sqrt{m}(1-v_c)]r^2\}(1-v_c)r^{-\sqrt{m}}d_s(t)}{\Delta}$$

(26)

$$c_4(r) = -\frac{\{(1-v_c)(\sqrt{m}-1)r^2 + [1-v_c + \sqrt{m}(1+v_c)]b^2\}(1+v_c)r^{\sqrt{m}}d_s(t)}{\Delta}$$

(27)

where

$$\begin{aligned}\Delta = &(1-v_c^2)(1-\sqrt{m})[(a/r)^{\sqrt{m}}b^2 + (r/a)^{\sqrt{m}}r^2]\\&-[(1-v_c^2)+\sqrt{m}(1+v_c)^2](r/a)^{\sqrt{m}}b^2\\&-[(1-v_c^2)+\sqrt{m}(1-v_c)^2](a/r)^{\sqrt{m}}r^2\end{aligned}$$

(28)

here v_c is Poisson's ratio of the concrete. Because $d_s(t)$ is a function of the corrosion rate, $i_{corr}(t)$, the thickness of the corrosion products can be expressed by substituting Equation (16) into Equation (15) as follows:

$$d_s(t) = \frac{0.81\sqrt{\dfrac{D_0}{\alpha_{rust}}\int_0^t i_{corr}(t)dt}}{\alpha_{rust}(D_0+2d_0)}\left(\frac{1}{\rho_{rust}} - \frac{\alpha_{rust}}{\rho_{st}}\right)$$

(29)

Substituting Equations (22) and (23) into Equation (21) and using the newly developed $i_{corr}(t)$ (Equation (13)) in Equation (29) for c_1, c_2, c_3, and c_4, the stiffness degradation factor, α, can be determined as follows:

$$\alpha = \frac{f_t e^{-\gamma\left(\frac{E_{ef}(b^{\sqrt{m}}-a^{\sqrt{m}})[c_3(b)+c_4(b)/(ab)^{\sqrt{m}}]}{\sqrt{m}(b-a)} - \frac{1}{b-a}\left(\int_a^b c_1(r)+\frac{c_2(r)}{r^2}dr\right)\right)}}{E_{ef}\dfrac{(b^{\sqrt{m}}-a^{\sqrt{m}})[c_3(b)+c_4(b)/(ad_c)^{\sqrt{m}}]}{\sqrt{m}(b-a)}}$$

(30)

Because this concrete stiffness degradation factor α is dependent on c_1, c_2, c_3, and c_4 and c_1, c_2, c_3, and c_4 are functions of corrosion rate, $i_{corr}(t)$, the concrete stiffness degradation factor can be directly related to corrosion rate, $i_{corr}(t)$. Therefore, the proposed corrosion rate model developed in this paper can be used to calculate the concrete stiffness degradation factor, α, and this can be used to predict the loss of capacity of a structure exhibiting corrosion of the reinforcement.

Three different levels of corrosion rates are considered in this study: low, moderate, and high as reported by Andrade et al. (2004) and shown in Figure 12. Figure 13 shows the concrete cover stiffness degradation factors as a function of time using the proposed corrosion rate model in Equation (13) for different corrosion levels. In this figure the concrete cover depth is assumed to be 51 mm (2 in.). Note that the stiffness of the concrete cover can be reduced by over 60% within a 10 year period for high corrosion rate. The next section will address how the capacity loss of the steel reinforcement and concrete cover stiffness loss as a result of corrosion of the reinforcement impact the lateral capacity of a column.
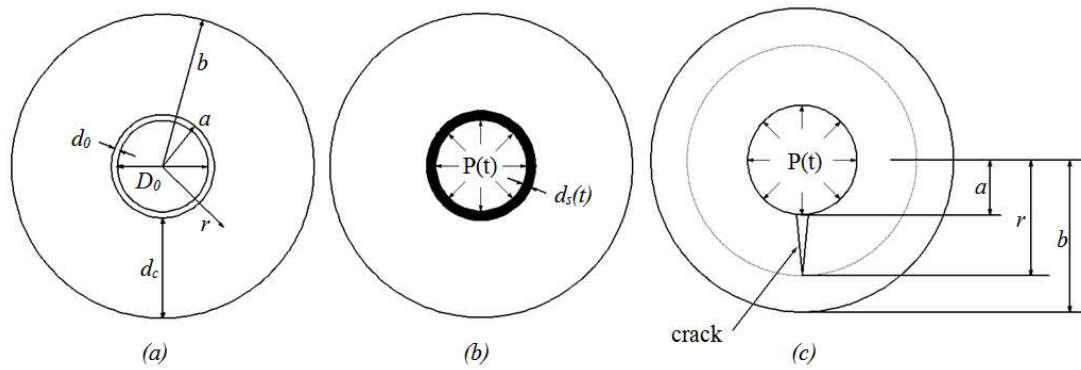
Figure 10. Schematic of corrosion-induced concrete cracking process: *(a)* thick-wall cylinder model; *(b)* a ring of corrosion products forms; *(c)* inner cracked and outer uncracked
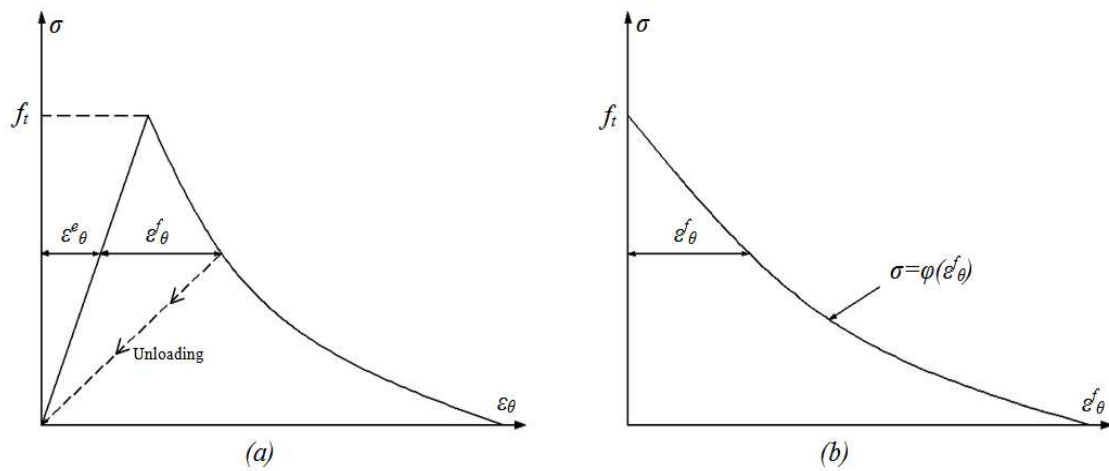
Figure 11. *(a)* elastic-softening stress strain curve; *(b)* stress-cracking strain curve
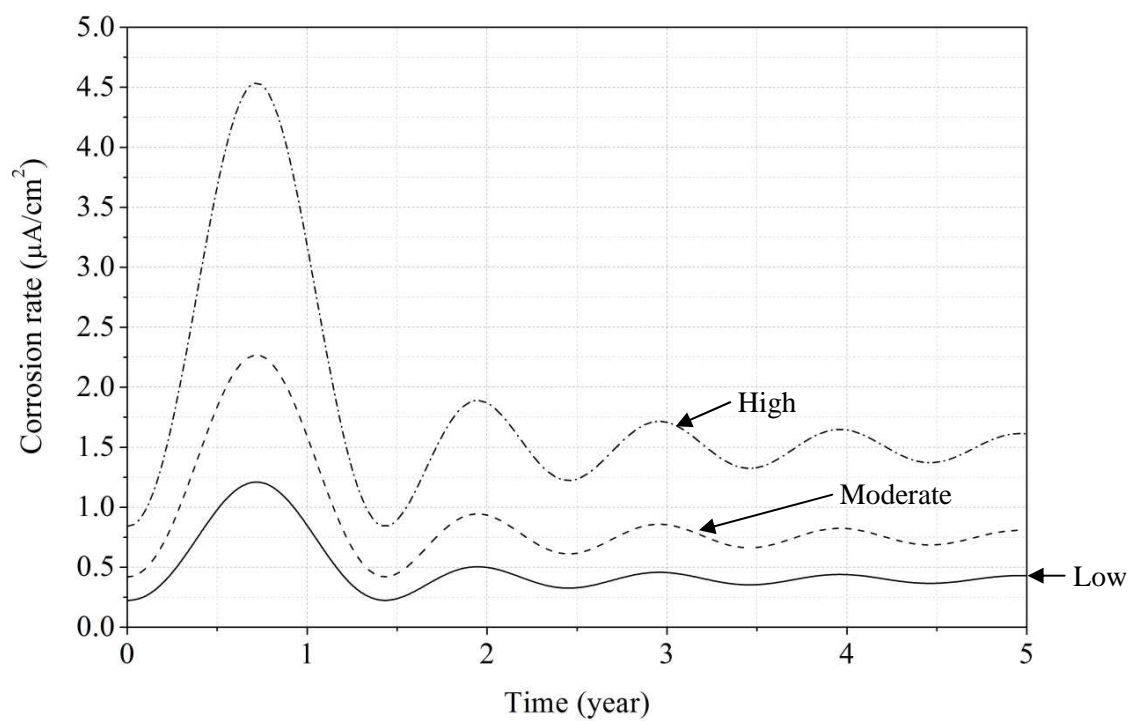
Figure 12. Low, moderate, and high corrosion levels
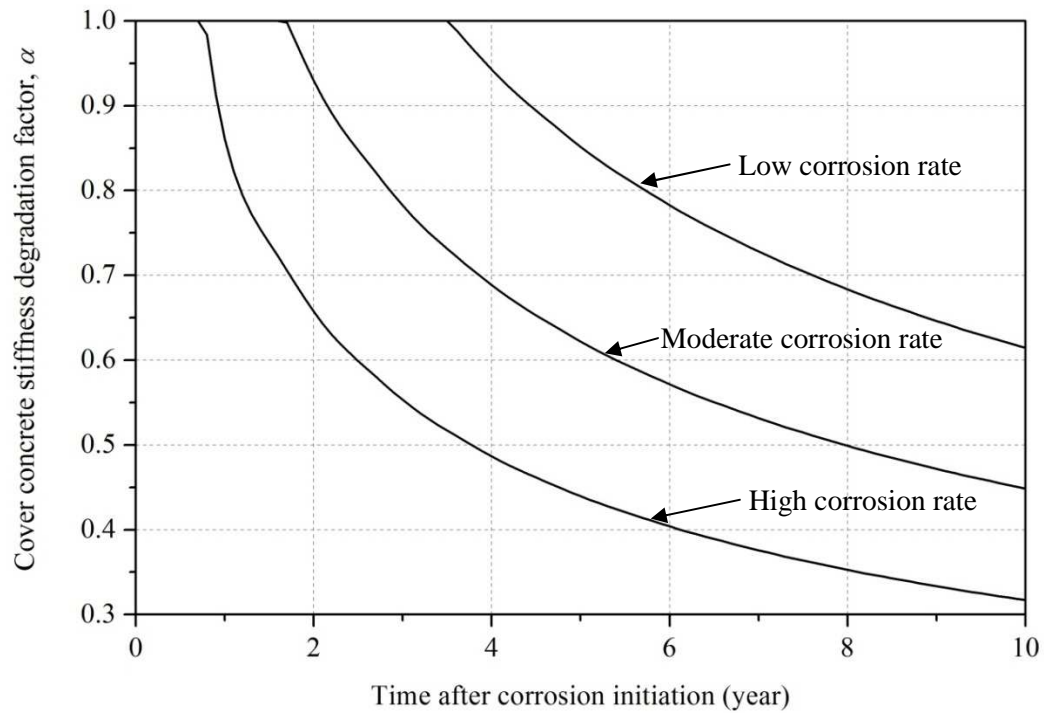
Figure 13. Concrete cover stiffness degradation factor

RELIABILITY ANALYSIS FOR CORRODED RC COLUMNS SUBJECT TO SEISMIC EVENT

A parametric study will be performed to assess the capacity of a corroding column subjected to a seismic event using the models developed. The column design represents an existing highway bridge column built in the early 1970s in the Northwest US. The modern seismic code was introduced in the early 1970s and the example bridge column was designed without the modern seismic code, which may make the RC structures and members more vulnerable to seismic induced damage. This analysis will assess the time-variant reliability of the corroding column.

The column details are shown in Figure 14. The diameter of the example column is 660 mm (26 in.) and the height is 5.49 m (18 ft). The column is reinforced with 8 #25M (#8) longitudinal steel bars and #16M (#5) spiral steel bars spaced at 127 mm (5 in.). The concrete compressive strength, f_c', is 24.8 MPa (3.6 ksi) and the reinforcing steel is grade 60 (f_y = 413.7 MPa (60 ksi)). The gross area (A_g) of the column is 3425 cm^2 (530.9 in.^{2}), the core area (A_{ch}) is 2623 cm^2 (406.5 in.^{2}), the steel area (A_{st}) is 40.5 cm^2 (6.3 in.^{2}), and reinforcement ratio A_{st}/A_g is 0.012. This probability analysis contains 19 random variables and the values are provided in Table 2.

The Open System for Earthquake Engineering Simulation (OpenSees) is used to simulate the seismic response and estimate the failure probability of the example column under seismic loads. OpenSees is a comprehensive, open-source, object-oriented software framework for simulating the seismic response of structural and geotechnical systems. OpenSees has previously been extended with reliability and response sensitivity capabilities. The program has a large library of elements and the element employed for the nonlinear analysis in this paper is identified as a nonlinear beam column. This nonlinear beam column is based on a fiber model and takes P-delta effects into consideration.

The example column is modeled using fiber sections with the uniaxial inelastic materials defined independently for different fibers. Basic assumptions of the fiber model include the plane section assumption, fully bonded fibers and no relative slip, and the model ignores shear deformation. The fiber section model divides the element section into distinct components. The stress-strain relationship of the overall section can be calculated using the uniaxial stress-strain relationship of the fibers. The core concrete of the example column is divided into 40 fibers and the concrete cover is divided into 16 fibers as shown in Figure 16. The numbers of fibers were determined to be sufficient, because increasing the number of the fibers by 100% only led to a 2.1% difference in the elastic stiffness and a 2.3% difference in the apparent yield point. One reinforcing bar is considered to be a fiber in this analysis. The model assumes the stress-strain relationship of concrete cover using the model developed by Kent and Park (1971). The model also assumes that the maximum stress, f'_{cc}, the ultimate stress, f'_{cu}, and the stiffness of the concrete cover decrease with time as shown in Figure 15. Here, ε_{cc} is the strain at maximum stress, f'_{cc}, and ε_{cu} is the strain at ultimate stress, f'_{cu}. The fiber section properties are listed in Table 3.

The probability of failure for the column was determined using Monte Carlo Simulation (MCS) with 10,000 iterations. MCS with 20,000 and 30,000 iterations were also performed to verify the

accuracy of the analysis. The iteration number of 10,000 was determined to be sufficient because the larger number of iterations resulted in an insignificant change in the results. The limit state function used in the MCS is discussed next.

Limit State Function of Column Failure

After the longitudinal reinforcement in the column yields, the column continues to undergo further lateral drift (i.e., plastic deformation) until the moment demand exceeds its moment capacity. When the column's moment capacity is exceeded, flexure failure occurs and the axial load capacity decreases. In this probabilistic analysis, failure of the columns under a seismic event will be defined as the point when the bending moment caused by the seismic load exceeds the moment capacity at the column bottom. The limit state function can be expressed as:

$$g(t, \mathbf{x}) = C_M(t, \mathbf{x}) - D_M \tag{31}$$

where $C_M(t, \mathbf{x})$ is the time-variant moment capacity of column and D_M is the moment demand at the column bottom. The vector $\mathbf{x}$ of random variables is written as:

$$\mathbf{x} = (D_{col}, D_0, f'_c, f_y, T_{mean}, T_{high}, T_{low}, w/c, Cl, Cl_{Th}, mc) \tag{32}$$

and the values of the random variables are provided in Table 2. The calculation of the moment capacity and demand are discussed in the following section.

Moment Capacity and Demand

An axial load is applied at the top of the column and is a result of dead and live loads. The moment capacity can be obtained from the axial load-moment (P-M) interaction. The P-M interaction is calculated using the fiber section model in OpenSees for the example column. For different times and corrosion rates after corrosion initiation, the diameter of steel bars and the concrete material properties change based on Equations (14) and (30) and both equations are functions of the corrosion rate. Therefore, the moment capacity is affected by the corrosion rate. The proposed corrosion rate model in Equation (13) is used to determine the time-variant moment capacity. The moment capacity is calculated using MCS and the values in Table 2.

A postulated earthquake event with a mean return period of 1000 years is used for the failure probability analysis. The intensity of the specified seismic event is characterized by effective

peak acceleration and the peak acceleration is obtained from the design response spectrum. The design response spectrum is generated for a highway located near Portland, OR with a site class D (stiff soil). The mapped spectral accelerations used to generate the design response spectrum were obtained from U.S. Geological Survey (USGS) website (www.usgs.gov accessed on September 2, 2011). Figure 17 shows the design response spectrum. Preliminary calculations indicate that the time-variant period for the example column will range from 0.65 to 0.75 seconds and a peak acceleration of 0.636 g will be used for this study. The demand seismic load is defined as the peak acceleration times the dead weight (3029 kN or 681 kips) of the superstructure applied at the top of the column.

Failure Probability and Reliability Index of Example Column

Different variables are used for the reliability analysis: corrosion level, concrete cover depth, and reinforcing steel bar size. For the reliability analysis with different corrosion levels, the other variables are kept the same as in Table 2. For the reliability analysis with different concrete cover depths and reinforcing steel bar sizes, the corrosion level is high and the other variables are kept the same as in Table 2.

Figure 18 shows the results of the probabilistic analysis for the three different corrosion levels. The results indicate that the failure probability increases significantly as a result of corrosion. To compare the reliability of the example column with the requirements of design codes, the failure probability is converted to the equivalent reliability index, β. A target reliability index of 3.5 is required by the AASHTO Load and Resistance Factor Design (LRFD) for new bridge structures and a target reliability index of 2.5 is required by the AASHTO Load and Resistance Factor Rating (LRFR) for existing bridge structures. Results indicate that the uncorroded structure subjected to a peak ground response acceleration of 0.636 g has reliability index, β, of slightly less than that required by AASHTO. The figure also shows that corrosion rate can significantly reduce the time-variant reliability of the columns.

Figure 19 shows the results of three different concrete cover depths for high corrosion level. The results indicate that the concrete cover depth affects the failure probability significantly. The increase of concrete cover depth leads to increase of the time to crack to concrete cover and decrease of the reliability index after the concrete cover spalls off.

Figure 20 shows the results of three different reinforcing steel bar sizes for high corrosion level. Because increasing the reinforcing steel bar size increases the capacity of the example column, the original reliability index without corrosion can then be increased. To compare the results with different original reliability index, the reliability index ratio is used here and defined as β/β_0. The results indicate that the reinforcing steel bar size affects the failure probability significantly and the increase of the reinforcing steel bar size increases the reliability index ratio of the columns subjected to corrosion. This increase is likely from the increase of longitudinal reinforcement ratio, which is defined as the area of the longitudinal reinforcing steel over the area of the cross section of the column, because the corrosion has more effect on the degradation of concrete cover than reinforcing steel.

Table 2. Random variables for the example column failure probability analysis under seismic load

Variables	Mean	COV	Distribution	Source
Original bar diameter, D_0 (mm)	25.4	0.05	Lognormal	Mirza et al. (1979)
Thickness of annular layer of concrete pores, d_0 (mm)	0.0125	0.05	Normal	Liu and Weyers (1998)
Corrosion products type coefficient, α_{rust} *	0.523-0.622	–	–	Liu and Weyers (1998)
Poison's ratio, v_c	0.18	0.05	Normal	Liu and Weyers (1998)
Effective elastic modulus of concrete, E_{ef} (MPa)	18,820	0.05	Normal	Li (2003)
Tensile strength of concrete, f_t (MPa)	5.725	0.05	Normal	Li (2003)
Density of corrosion products, ρ_{rust} (mg/mm^3)	3.6	0.05	Normal	Liu and Weyers (1998)
Density of steel, ρ_{st} (mg/mm^3)	7.85	0.05	Normal	Liu and Weyers (1998)
Material constant, γ	1.3	–	–	Li et al. (2006)
Ratio between the Poisson's ratios in the tangential and radial directions, m	1	–	–	Li et al. (2006)
Column diameter, D_{col} (mm)	660	0.05	Lognormal	Mirza et al. (1979)
Compressive stress of concrete, f'_c (Mpa)	24.82	0.1	Lognormal	Mirza et al. (1979)
Steel yield strength, f_y (Mpa)	413.7	0.05	Beta	Mirza et al. (1979)
Annual mean temperature, T_{mean} (K)	285.1	0.05	Normal	DuraCrete (2000)
Average high temperature, T_{high} (K)	289.9	0.05	Normal	DuraCrete (2000)
Average low temperature, T_{low} (K)	280.3	0.05	Normal	DuraCrete (2000)
Water-cement ratio, w/c	0.45	0.05	Lognormal	DuraCrete (2000)
Chloride concentration, Cl (kg/m^3)	1.45	0.2	Normal	DuraCrete (2000)
Chloride threshold concentration, Cl_{Th} (kg/m^3)	1.45	0.2	Normal	DuraCrete (2000)
Moisture content, mc	0.75	0.2	Normal	DuraCrete (2000)
Axial load, P_{axial} (kN)	5276	0.1	Lognormal	–

*Assume the composition of rust products is between $Fe(OH)_3$ and $Fe(OH)_2$ α_{rust} varies from 0.523 to 0.622

Table 3. Material parameters of the concrete material

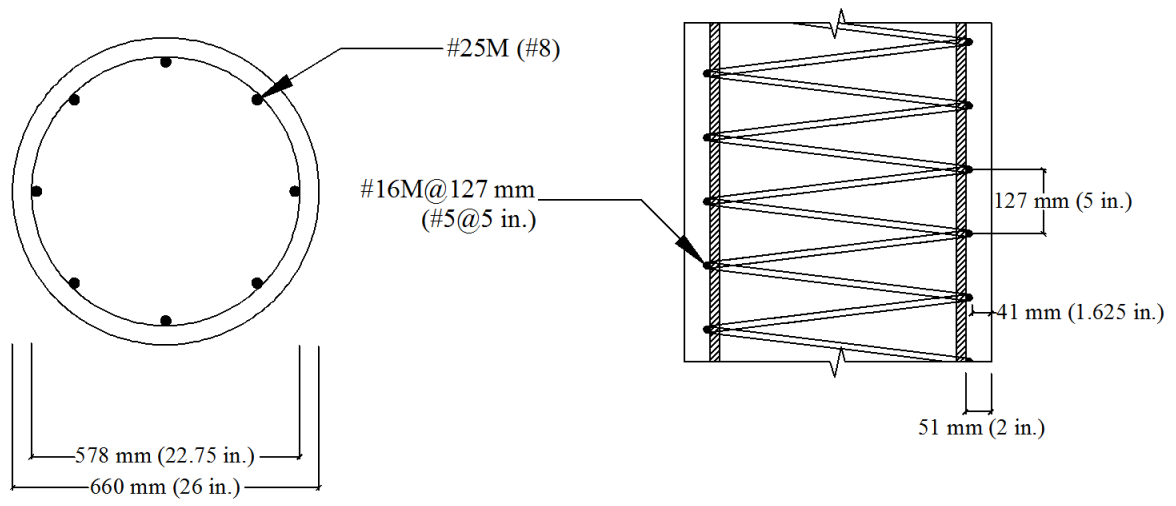|	Cover	Core
Compressive Strength (MPa or psi)	f'_c	f'_c
Concrete Elastic Modulus (MPa or psi)	$4700\sqrt{f'_c}$ or $57,000\sqrt{f'_c}$	$4700\sqrt{f'_c}$ or $57,000\sqrt{f'_c}$
Maximum stress (MPa or psi)	$\alpha f'_c$	$1.3 f'_c$
Strain at maximum stress	0.003	$\dfrac{2f'_c}{E_c}$
Ultimate stress (MPa or psi)	$0.2\,\alpha f'_c$	$0.26 f'_c$
Strain at ultimate stress	0.001	$\dfrac{10f'_c}{E_c}$

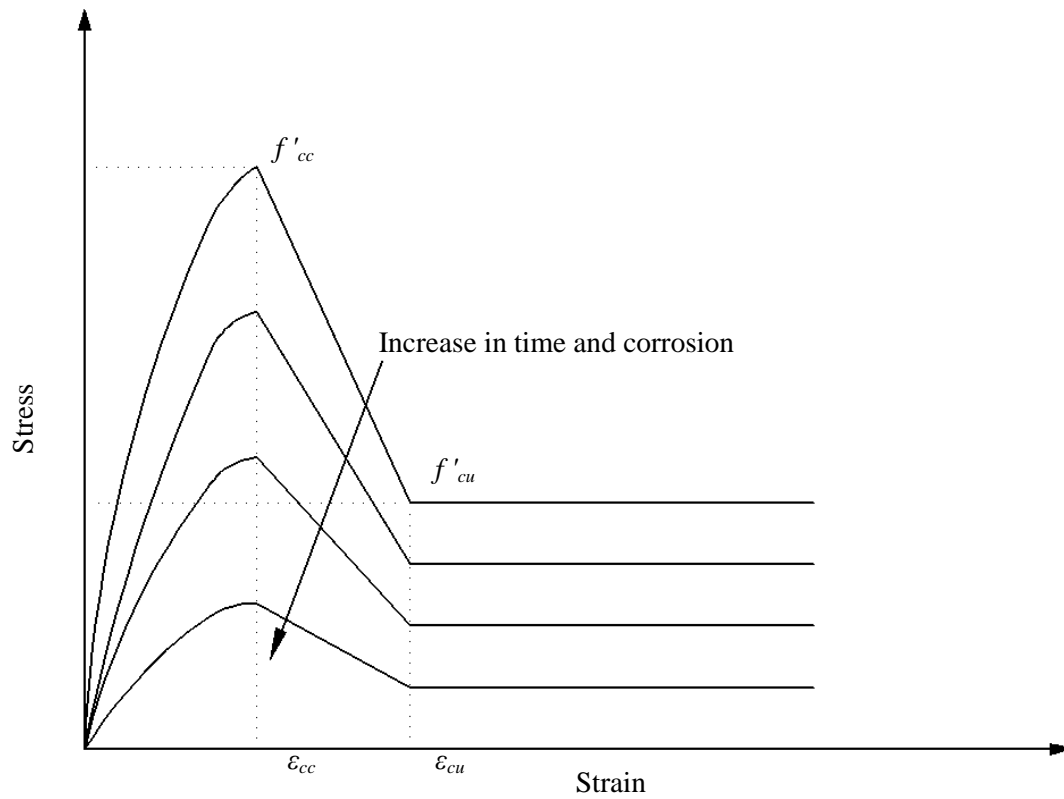Figure 14. Dimensions of example column

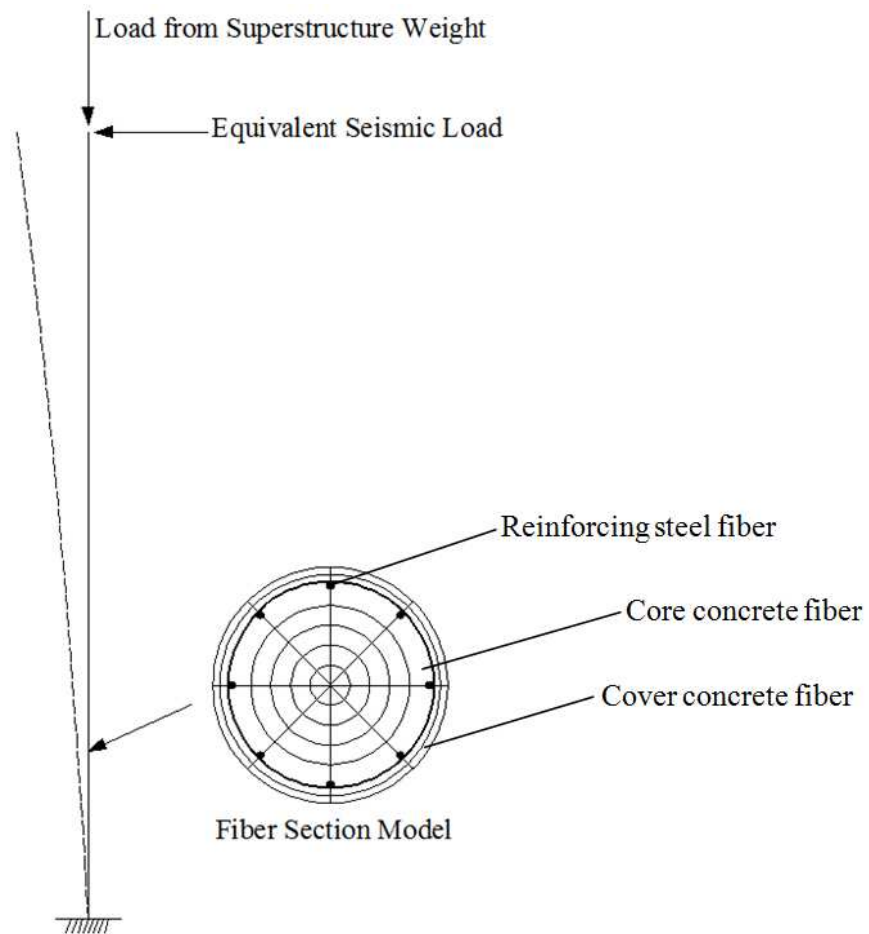Figure 15. Changes in stress-strain relationship as a function of time and corrosion

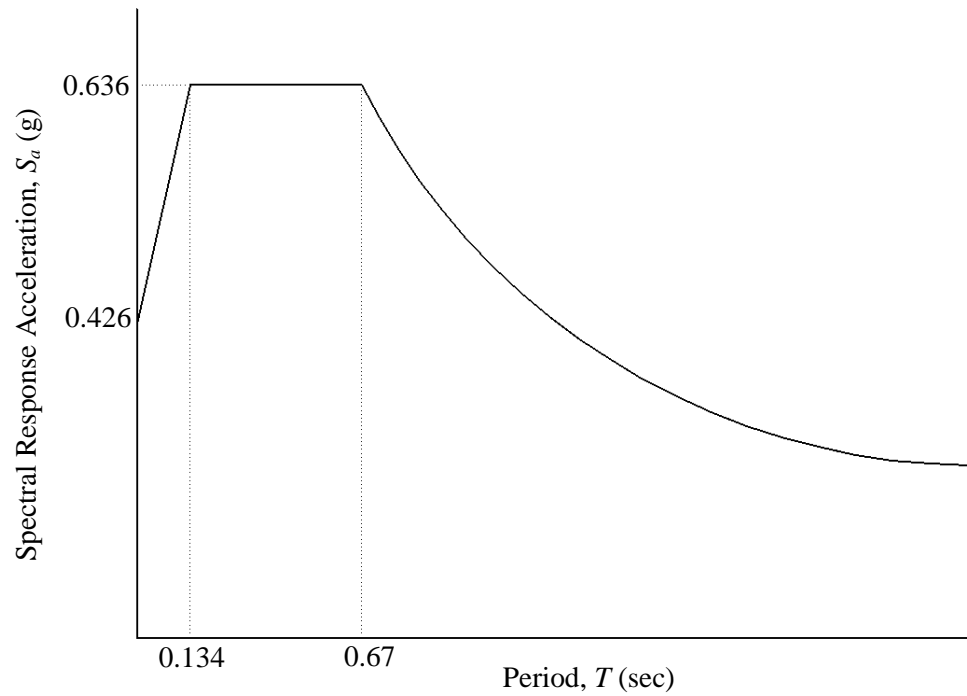Figure 16. OpenSees model showing fibers, loads, and integration points

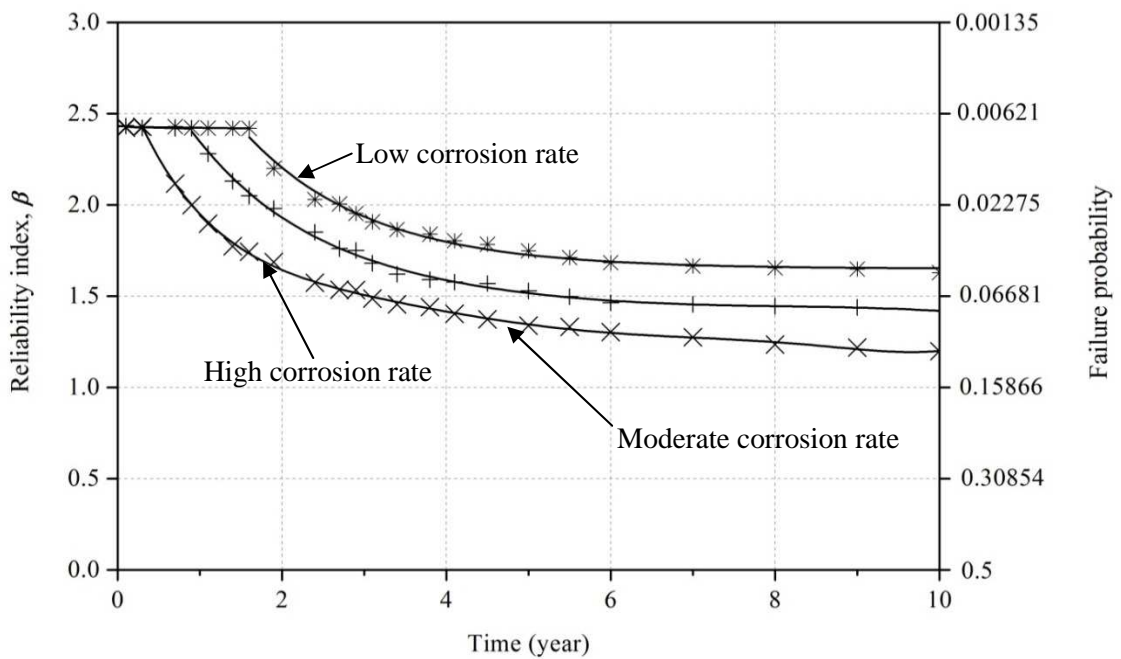Figure 17. Design response spectrum

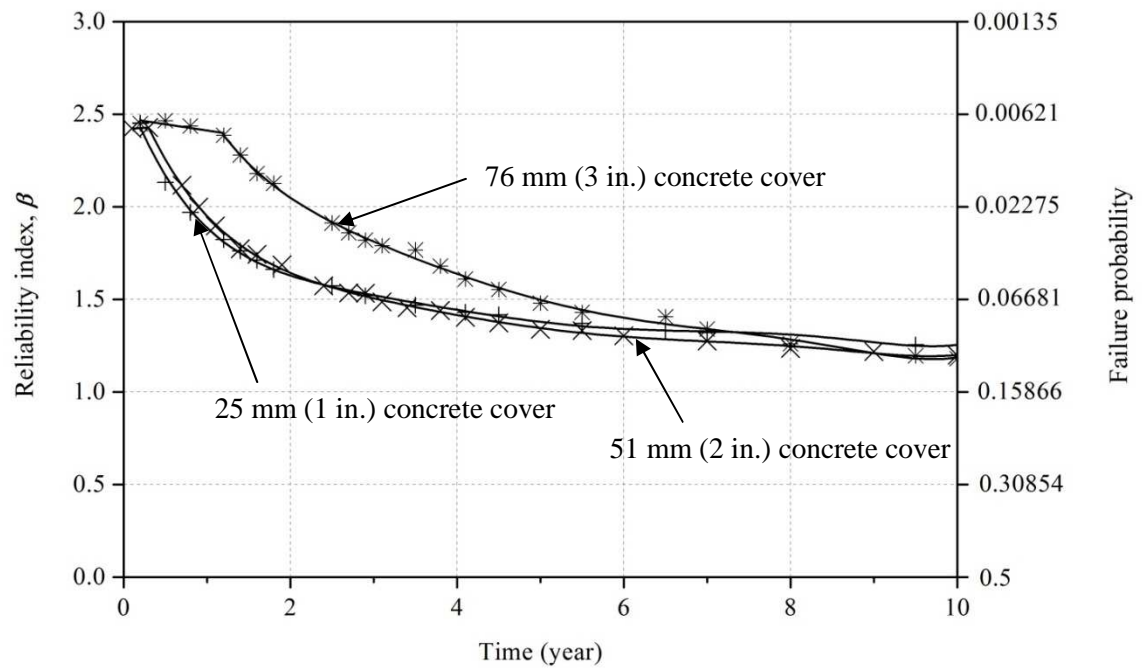Figure 18. Failure probability of example column subject to seismic event

Figure 19. Failure probability of example column for different concrete covers
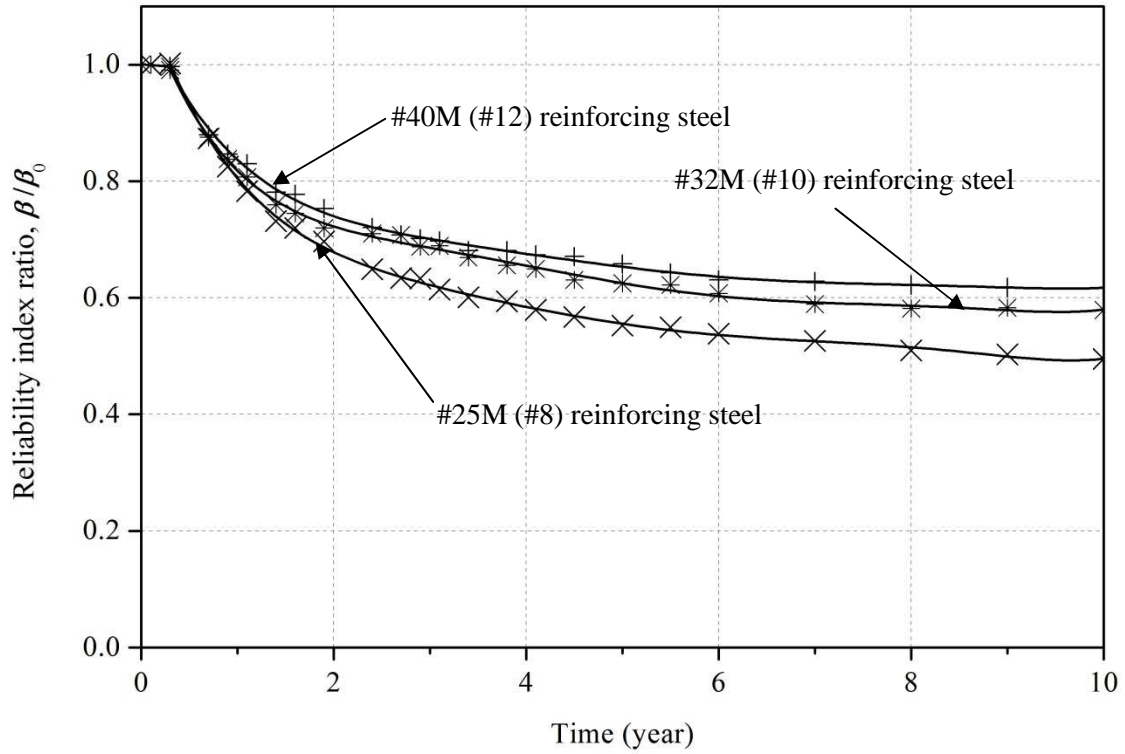
Figure 20. Failure probability of example column for different reinforcing steel bar sizes

CONCLUSION

This paper presents a critical review of existing models used to predict the corrosion rate of steel reinforcement in RC structures. The review indicates that the existing models reported in the literature do not consider influencing factors and do not represent actual measured corrosion rates or trends. A new time-variant corrosion rate model for chloride-induced corrosion was developed. The proposed model incorporates influencing variables for modeling the corrosion propagation phase, such as of the moisture content, the chloride concentration, the concrete characteristics, the annual mean temperature, and the seasonal temperature changes. Results indicate that the proposed corrosion rate model better represents actual measured corrosion rates than the existing

models evaluated and can therefore better represent the effects of corrosion on the performance of RC structures. This new corrosion rate model can be used to evaluate the residual load-carrying capacity of existing structures. This research found that the time-variant corrosion rate, the concrete cover, and the reinforcing steel bar size have significant influences on the lateral capacity of a column subjected to the seismic event presented herein. Results indicate that a significant increase in probability of failure occurs within the first couple of years of the corrosion initiation. After the first couple of years, the rate of probability of failure decreases at a nearly constant value. The results also indicate that the reliability of the example column is lower than the requirement of AASHTO LRFR.

NOTATIONS

a	Inner radius of the thick-wall cylinder, mm (in.)
a_s	Corrosion initiation season factor
A_{ch}	Core area the column, mm^2 (in^2)
A_g	Gross area of the column, mm^2 (in^2)
A_{st}	Steel area the column, mm^2 (in^2)
b	Outer radius of the thick-wall cylinder, mm (in.)
c_1, c_2, c_3, c_4	Parameters used to calculate the stiffness degradation factor of concrete cover
Cl	Chloride concentration in concrete, kg/m^3 (lb/ft^3)
Cl_{Th}	Chloride threshold of steel reinforcement, kg/m^3 (lb/ft^3)
$C_M(t, \mathbf{x})$	Time-variant moment capacity of column, kN-m (k-ft)
C_s	Chloride concentration on the concrete surface, kg/m^3 (lb/ft^3)
d_0	Thickness of annular layer of concrete pores, mm (in.)
$d_s(t)$	Thickness of the corrosion products, mm (in.)
D_0	Original steel reinforcing bar diameter, mm (in.)
D_a	Apparent diffusion coefficient of concrete, cm^2/s (in^2/s)
D_{col}	Column diameter, mm (in.)
D_M	Moment demand at the column bottom, kN-m (k-ft)
$D(t)$	Reduced diameter of the reinforcing bar at some time, mm (in.)
E_{ef}	Effective elastic modulus of concrete, MPa (psi)
E_θ	Tangential elastic modulus of concrete for unloading, MPa (psi)
f_t	Tensile strength of concrete, MPa (psi)
f'_c	Compressive strength at 28 day of concrete, MPa (psi)
f'_{cc}	Maximum strength at 28 day of concrete, MPa (psi)
f'_{cu}	Ultimate strength at 28 day of concrete, MPa (psi)
f_y	Steel yield strength, MPa (psi)

f_{O_2}	Oxygen concentration factor
f_{mc}	Moisture content factor
f_{res}	Concrete resistivity factor
$f_{w/c}$	Water-to-cement ratio factor
f_{d_c}	Concrete cover depth factor
f_T	Temperature factor
f_{Cl}	Chloride concentration factor
$f_{T_{mean}}$	Annual mean temperature factor
$f_{T_{seasonal}}$	Seasonal temperature factor
$i_{corr,0}$	Basic corrosion rate, $\mu A/cm^2$ ($\mu A/ft^2$)
i_{corr}	Corrosion rate, $\mu A/cm^2$ ($\mu A/ft^2$)
m	Ratio between the Poisson's ratios in the tangential and radial directions
mc	Moisture content, %
P_{axial}	Axial load, kN (kip)
r	Distance from any point to the centroid of the cross section of the reinforcing bar, mm (in.)
R_c	Ohmic resistance of the concrete cover, ohm
t	Time, year
T_{mean}	Annual mean temperature, K (°F)
T_{high}	Average high temperature, K (°F)
T_{low}	Average low temperature, K (°F)
w/c	Water-cement ratio
$W_{rust}(t)$	Mass of corrosion products, g (lb)
x	Distance from any point inside the concrete to the surface, mm (in.)
$\mathbf{x}$	Vector of random variables

α	Stiffness degradation factor of concrete cover
α_{rust}	Corrosion products type coefficient
β_0	Original reliability index before corrosion initiation
β	Equivalent reliability index
γ	Material constant
ε_{cc}	Strain at maximum stress of concrete
ε_{cu}	Strain at ultimate stress of concrete
ε_θ	Total tangential strain across crack
ε_θ^e	Elastic tangential strain across crack
ε_θ^f	Actual cracking strain across crack
ρ_{rust}	Density of corrosion products, mg/mm^3 (lb/ft^3)
ρ_{st}	Density of steel, mg/mm^3 (lb/ft^3)
σ	Cohesive stress
v_c	Poison's ratio

BIBLIOGRAPHY

Ahmad, S. (2003). "Reinforcement corrosion in concrete structures, its monitoring and service life prediction - a review." *Cement & Concrete Composites* 25(4-5): 459-471.

Ahmad, S. and Bhattacharjee, B. (2000). "Empirical Modeling of Indicators of Chloride-Induced Rebar Corrosion." *Journal of Structural Engineering, Chennai (India)* 27(3): 195-207.

Alonso, C., Andrade, C. and Gonzalez, J. A. (1988). "Relation between Resistivity and Corrosion Rate of Reinforcements in Carbonated Mortar Made with Several Cement Types." *Cement and Concrete Research* 18(5): 687-698.

Alonso, C., Andrade, C., Rodriguez, J. and Diez, J. M. (1998). "Factors controlling cracking of concrete affected by reinforcement corrosion." *Materials and Structures* 31(211): 435-441.

American Association of State Highway and Transportation Officials. (2007). AASHTO LRFD bridge design specifications, customary U.S. units. Washington, DC, American Association of State Highway and Transportation Officials.

Andrade, C., Alonso, C., Gulikers, J., Polder, R., Cigna, R., Vennesland, O., Salta, M., Raharinaivo, A. and Elsener, B. (2004). "Test methods for on-site corrosion rate measurement of steel reinforcement in concrete by means of the polarization resistance method." *Materials and Structures* 37(273): 623-643.

Andrade, C., Alonso, C. and Molina, F. J. (1993). "Cover Cracking as a Function of Rebar Corrosion: Part I - Experimental Test." *Materials and Structures* 26: 453-464.

Böhni, H. (2005). Corrosion in reinforced concrete structures. CRC Press.

Balabanic, G., Bicanic, N. and Durekovic, A. (1996). "The influence of w/c ratio, concrete cover thickness and degree of water saturation on the corrosion rate of reinforcing steel in concrete." *Cement and Concrete Research* 26(5): 761-769.

Balafas, I. and Burgoyne, C. J. (2010). "Environmental effects on cover cracking due to corrosion." *Cement and Concrete Research* 40(9): 1429-1440.

Bazant, Z. P. (1979). "Physical Model for Steel Corrosion in Concrete Sea Structures - Application." *Journal of the Structural Division-Asce* 105(6): 1155-1166.

Bertolini, L., Elsener, B., Pedeferri, P. and Polder, R. (2004). Corrosion of Steel in Concrete: Prevention, Diagnosis, Repair. Weinheim, Wiley-VCH.

Broomfield, J. P. (1997). Corrosion of steel in concrete : understanding, investigation, and repair. London ; New York, E & FN Spon.

Choe, D. E., Gardoni, P., Rosowsky, D. and Haukaas, T. (2009). "Seismic fragility estimates for reinforced concrete bridges subject to corrosion." *Structural Safety* 31(4): 275-283.

DuraCrete (2000). Brite EuRam: DuraCrete – Final Technical Report. DuraCrete – Probabilistic Performance based Durability Design of Concrete Structures. Brussel, Contract BRPR-CT95-0132, Project BE95-1347, Document BE95-1347/R17.

DuraCrete. (2000). Statistical quantification of the variables in the limit state functions: summary. Document BE95-1347/R9, Brite EuRam III, CUR, Gouda.

Fang, C. Q., Lundgren, K., Chen, L. G. and Zhu, C. Y. (2004). "Corrosion influence on bond in reinforced concrete." *Cement and Concrete Research* 34(11): 2159-2167.

Hussain, S. E., Rasheeduzzafar, Almusallam, A. and Algahtani, A. S. (1995). "Factors Affecting Threshold Chloride for Reinforcement Corrosion in Concrete." *Cement and Concrete Research* 25(7): 1543-1555.

Jones, D. A. (1996). Principles and prevention of corrosion. Upper Saddle River, NJ, Prentice Hall.

Kobayashi, K. and Shuttoh, K. (1991). "Oxygen Diffusivity of Various Cementitious Materials." *Cement and Concrete Research* 21(2-3): 273-284.

Koch, G. H., Brongers, P. H., Thompson, N. G., Virmani, Y. P. and Payer, J. H. (2002). Corrosion Costs and Prevention Strategies in the United States. Report No. FHWA-RD-01-156. Washington, DC., Federal Highway Administration.

Li, C. Q. (2004). "Reliability based service life prediction of corrosion affected concrete structures." *Journal of Structural Engineering-Asce* 130(10): 1570-1577.

Li, C. Q., Melchers, R. E. and Zheng, J. J. (2006). "Analytical model for corrosion-induced crack width in reinforced concrete structures." *ACI Structural Journal* 103(4): 479-487.

Liu, T. and Weyers, R. W. (1998). "Modeling the dynamic corrosion process in chloride contaminated concrete structures." *Cement and Concrete Research* 28(3): 365-379.

Liu, Y. P. and Weyers, R. E. (1998). "Modeling the time-to-corrosion cracking in chloride contaminated reinforced concrete structures." *ACI Materials Journal* 95(6): 675-681.

Lopez, W. and Gonzalez, J. A. (1993). "Influence of the Degree of Pore Saturation on the Resistivity of Concrete and the Corrosion Rate of Steel Reinforcement." *Cement and Concrete Research* 23(2): 368-376.

Martinez, I. and Andrade, C. (2009). "Examples of reinforcement corrosion monitoring by embedded sensors in concrete structures." *Cement & Concrete Composites* 31(8): 545-554.

Mirza, S. A., MacGregor, J. G. and Hatzinikolas, M. (1979). "Statistical Descriptions of Strength of Concrete." *Journal of the Structural Division-Asce* 105(6): 1021-1037.

Morris, W., Vico, A. and Vazquez, M. (2004). "Chloride induced corrosion of reinforcing steel evaluated by concrete resistivity measurements." *Electrochimica ACTA* 49(25): 4447-4453.

Neville, A. M. (1996). Properties of Concrete: Fourth Edition, Wiley.

Otieno, M. B., Beushausen, H. D. and Alexander, M. G. (2011). "Modelling corrosion propagation in reinforced concrete structures - A critical review." *Cement and Concrete Composites* 33(2): 240-245.

Pour-Ghaz, M., Isgor, O. B. and Ghods, P. (2009). "The effect of temperature on the corrosion of steel in concrete. Part 1: Simulated polarization resistance tests and model development." *Corrosion Science* 51(2): 415-425.

Simon, J., Bracci, J. M. and Gardoni, P. (2010). "Seismic Response and Fragility of Deteriorated Reinforced Concrete Bridges." *Journal of Structural Engineering-Asce* 136(10): 1273-1281.

Song, H. W. and Saraswathy, V. (2007). "Corrosion monitoring of reinforced concrete structures - A review." *International Journal of Electrochemical Science* 2(1): 1-28.

Stewart, M. G. and Rosowsky, D. (1998). "Structural safety and serviceability of concrete bridges subject to corrosion." *Journal of Infrastructure Systems* 4(4).

Thomas, M. D. A. and Bentz, E. C. (2002). "Life-365 Product Manual: Computer Program for Predicting the Service Life and Life-cyle Costs of Reinforced Concrete Exposed to Chlorides."

Torres-Acosta, A. A. and Sagues, A. A. (2004). "Concrete cracking by localized steel corrosion - Geometric effects." *ACI Materials Journal* 101(6): 501-507.

Trejo, D. and Monteiro, P. J. (2005). "Corrosion performance of conventional (ASTM A615) and low-alloy (ASTM A706) reinforcing bars embedded in concrete and exposed to chloride environments." *Cement and Concrete Research* 35(3): 562-571.

Vu, K., Stewart, M. G. and Mullard, J. (2005). "Corrosion-induced cracking: Experimental data and predictive models." *ACI Structural Journal* 102(5): 719-726.

Vu, K. A. T. and Stewart, M. G. (2000). "Structural reliability of concrete bridges including improved chloride-induced corrosion models." *Structural Safety* 22(4): 313-333.

Wang, X. H. and Liu, X. L. (2004). "Modeling bond strength of corroded reinforcement without stirrups." *Cement and Concrete Research* 34(8): 1331-1339.

Yalçyn, H. and Ergun, M. (1996). "The prediction of corrosion rates of reinforcing steels in concrete." *Cement and Concrete Research* 26(10): 1593-1599.

Zhong, J. Q., Gardoni, P. and Rosowsky, D. (2010). "Stiffness Degradation and Time to Cracking of Cover Concrete in Reinforced Concrete Structures Subject to Corrosion." *Journal of Engineering Mechanics-ASCE* 136(2): 209-219.